

A new glacial isostatic adjustment model for Antarctica: calibrated and tested using observations of relative sea-level change and present-day uplift rates

Pippa L. Whitehouse,¹ Michael J. Bentley,¹ Glenn A. Milne,² Matt A. King³ and Ian D. Thomas³

¹Department of Geography, Durham University, South Road, Durham, DH1 3LE, UK. E-mail: pippa.whitehouse@durham.ac.uk

²Department of Earth Sciences, University of Ottawa, Marion Hall, Ottawa, Canada K1N 6N5

³School of Civil Engineering and Geosciences, Newcastle University, Newcastle upon Tyne, UK

Accepted 2012 May 24. Received 2012 April 12; in original form 2011 November 19

SUMMARY

We present a glacial isostatic adjustment (GIA) model for Antarctica. This is driven by a new deglaciation history that has been developed using a numerical ice-sheet model, and is constrained to fit observations of past ice extent. We test the sensitivity of the GIA model to uncertainties in the deglaciation history, and seek earth model parameters that minimize the misfit of model predictions to relative sea-level observations from Antarctica. We find that the relative sea-level predictions are fairly insensitive to changes in lithospheric thickness and lower mantle viscosity, but show high sensitivity to changes in upper mantle viscosity and constrain this value (95 per cent confidence) to lie in the range $0.8\text{--}2.0 \times 10^{21}$ Pa s. Significant misfits at several sites may be due to errors in the deglaciation history, or unmodelled effects of lateral variations in Earth structure. When we compare our GIA model predictions with elastic-corrected GPS uplift rates we find that the predicted rates are biased high (weighted mean bias = 1.8 mm yr^{-1}) and there is a weighted root-mean-square (WRMS) error of 2.9 mm yr^{-1} . In particular, our model systematically over-predicts uplift rates in the Antarctica Peninsula, and we attempt to address this by adjusting the Late Holocene loading history in this region, within the bounds of uncertainty of the deglaciation model. Using this adjusted model the weighted mean bias improves from 1.8 to 1.2 mm yr^{-1} , and the WRMS error is reduced to 2.3 mm yr^{-1} , compared with 4.9 mm yr^{-1} for ICE-5G v1.2 and 5.0 mm yr^{-1} for IJ05. Finally, we place spatially variable error bars on our GIA uplift rate predictions, taking into account uncertainties in both the deglaciation history and modelled Earth viscosity structure. This work provides a new GIA correction for the GRACE data in Antarctica, thus permitting more accurate constraints to be placed on current ice-mass change.

Key words: Satellite geodesy; Sea level change; Transient deformation; Rheology: mantle; Antarctica.

1 INTRODUCTION

Recent advances in the field of Antarctic glacial geology have generated renewed interest in reconstructing the past extent of the Antarctic Ice Sheet (AIS; Whitehouse *et al.* 2012, and references therein). These advances are not reflected in existing glacial isostatic adjustment (GIA) models and hence new models are required. GIA models describe the ongoing viscoelastic response of the solid Earth to past changes in surface loading by ice and water, and may be used to answer two key scientific questions.

First, GIA model output is largely governed by two inputs; the global ice-loading history and the rheology of the Earth. The former uniquely describes global changes in surface loading via solutions

to the sea-level equation (Farrell & Clark 1976), while the latter dictates the response of the Earth to these changes in surface loading. Within a GIA model, these two inputs are tuned to fit available field constraints relating to, for example, past ice extent, relative sea-level change and present-day uplift. In other words, the use of a GIA model permits consistent bounds to be placed on past ice-sheet changes and the rheological properties of the solid Earth. The recent availability of new field constraints from Antarctica has improved our ability to constrain these key inputs.

Secondly, the ongoing solid Earth response to past ice-mass change contaminates observations of present-day ice-mass change. In particular, the magnitude of the GIA contribution to secular changes in the Earth's gravitational field, as measured by the

Gravity Recovery and Climate Experiment (GRACE) satellites, is of the same order of magnitude as the contribution from present-day ice-mass change. The GIA signal is therefore typically modelled, and subtracted from the GRACE data, to reveal the magnitude and spatial distribution of current ice-mass change (Chen *et al.* 2006; Ramillien *et al.* 2006; Velicogna & Wahr 2006; Chen *et al.* 2008; Chen *et al.* 2009; Velicogna 2009). GIA modelling uncertainties presently dominate the GRACE error budget (Velicogna & Wahr 2006) and systematically bias ice mass balance estimates (Thomas *et al.* 2011), and therefore it is vital that these uncertainties be tightly constrained, and clearly documented.

Several Antarctic deglacial models have previously been published (Ritz *et al.* 2001; Huybrechts 2002; Peltier 2004; Ivins & James 2005; Pollard & DeConto 2009), but they vary widely in the amplitude and distribution of ice mass loss since the Last Glacial Maximum (LGM). This variance reflects the variety of methods and data used to construct these models, and suggests that errors in at least some of the models are large. The IJ05 (Ivins & James 2005) and ICE-5G (Peltier 2004) GIA models have been widely used to model the gravitational signature of GIA and hence correct GRACE data (Chen *et al.* 2006; Ramillien *et al.* 2006; Velicogna & Wahr 2006; Chen *et al.* 2008; Chen *et al.* 2009; Velicogna 2009). However, recent GPS studies have highlighted differences between direct observations of surface uplift and these models (Bevis *et al.* 2009; Argus *et al.* 2011; Thomas *et al.* 2011). Importantly, Thomas *et al.* (2011) showed that both models over-predict uplift at their local maxima, suggesting that there will be a systematic bias in subsequent GRACE-derived ice mass balance estimates. Riva *et al.* (2009) indirectly estimated GIA uplift from satellite altimetry and GRACE data, and produced an uplift field which has uniformly lower uplift rates compared with IJ05 and ICE-5G. Wu *et al.* (2010) empirically adjusted the IJ05 model using global geodetic data sets, and produced an estimate of uplift which does not appear to have substantially improved the unmodified model (Thomas *et al.* 2011). Observations of Antarctic relative sea-level (RSL) change also provide a test of GIA models (e.g. Nakada *et al.* 2000); such a test applied to the Huybrechts deglacial history (Huybrechts 2002) within a GIA model revealed a poor fit at several sites, indicating that this model also contains errors (Bassett *et al.* 2007).

GIA model errors have not previously been provided, adding to the uncertainty in the GIA contribution to GRACE data. In GRACE ice mass balance estimates this has led to the error remaining unquantified (Chen *et al.* 2006), or model differences being used to quantify model errors (e.g. Velicogna & Wahr 2006); neither approach accurately reflects the true uncertainty, especially considering that GIA model errors, when applied to GRACE data, result in systematic not random errors.

In this paper, we present a new GIA model for Antarctica, taking advantage of recent developments in the knowledge of ice history based on glacial geological and glaciological observations. In particular, we test a newly reconstructed deglaciation history for Antarctica (Whitehouse *et al.* 2012), which has been developed using the Glimmer ice sheet model (Rutt *et al.* 2009), and is tuned to fit observations of past ice extent (Whitehouse *et al.* 2012). The effect of ice model uncertainty is assessed using a suite of 16 plausible variants of the ice model. Uncertainty in the earth model parameters is quantified using a χ^2 test, and a preferred earth model is selected by fitting to near-field RSL data before comparing to recently published GPS uplift rates (see Fig. 1). Uncertainty in the model is further quantified by examining a set of perturbations to the ice-loading history. The output of this study is a new, error-bounded, GIA model for Antarctica, which can be used with GRACE data to

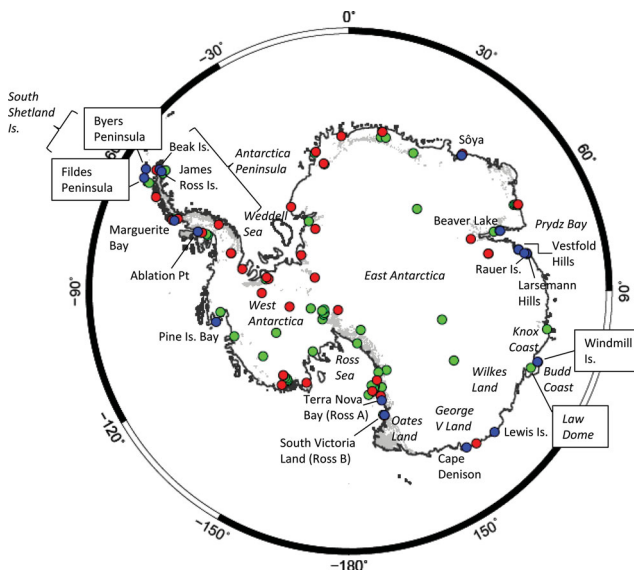


Figure 1. Location map for Antarctica. RSL sites are shown in blue, GPS sites are shown in red, and ice extent sites (Whitehouse *et al.* 2012) are shown in green. Rock outcrops are plotted in grey. Non-italicized labels refer to RSL (blue) sites; other sites mentioned in the text are labelled in italics.

produce more accurate estimates of present-day Antarctic ice-mass change.

2 MODEL DESCRIPTION

2.1 Reconstruction of the Antarctic ice sheet

A new Antarctic deglacial model (Whitehouse *et al.* 2012; subsequently referred to as the W12 model) is used to drive a GIA model. The W12 model was constructed using a numerical ice-sheet model (Rutt *et al.* 2009), and tuned to fit 62 glaciological and glacial geological constraints (see Fig. 1) relating to variations in the thickness and extent of the AIS since the LGM. The solid Earth response to loading, and the reconfiguration of the geoid, is determined by the change in the thickness of grounded ice at each time step. The total ice thickness at each time step is defined to be the sum of the present-day observed ice thickness (Le Brocq *et al.* 2010) and the change in W12 model ice thickness between that time step and the present-day (see Supporting Information). This preserves the changes in ice thickness derived using the numerical ice-sheet model; the metric that was used to tune the ice-sheet reconstruction in Whitehouse *et al.* (2012).

The W12 model is only defined at five specific time slices (20 ka BP, 15 ka BP, 10 ka BP, 5 ka BP and the present-day) because there are insufficient data to constrain a reconstruction at a higher temporal resolution (Whitehouse *et al.* 2012). However, a higher temporal resolution loading history is required to drive the GIA model to avoid large steps in loading, which may otherwise create model artefacts. To do this, we interpolate between the glaciologically consistent W12 time slices at 1 ka intervals, increasing to 500 yr intervals during periods of rapid deglaciation. Present-day ice-mass change is not taken into account in any variant of the model. Both lateral and vertical ice extent (see Supporting Information) are interpolated in four different ways (see Fig. 2)

- (1) linearly between the 5 ka configurations (model L);
- (2) in a ‘stepped’ manner (model S) guided by higher resolution

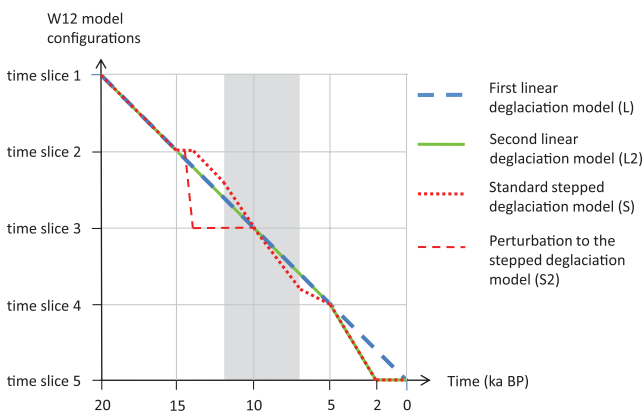


Figure 2. The rate of deglaciation between the W12 model configurations. See main text and Supporting Information for details of the four models. Time slice 1 = 20 ka BP reconstruction, time slice 2 = 15 ka BP reconstruction, time slice 3 = 10 ka BP reconstruction, time slice 4 = 5 ka BP reconstruction, time slice 5 = present-day reconstruction; time slice reconstructions are detailed in (Whitehouse *et al.* 2012). The vertical grey bar highlights the period of faster retreat in the stepped model (S), between 12 and 7 ka BP.

geological constraints on grounding line retreat (see Section S2.2, Supporting Information);

(3) with deglaciation identical to model L until 5 ka BP, but the final increment of retreat takes place linearly between 5 and 2 ka BP, with no ice mass change during the last 2 ka of the model (model L2);

(4) with deglaciation identical to model S except that all of the retreat from the W12 15 ka BP configuration to the W12 10 ka BP configuration is assumed to have occurred between 14.5 and 14 ka BP; the timing of melt water pulse 1A (Liu & Milliman 2004; model S2).

Note that since the 5 ka-spaced grounding lines are not equidistant, even the linear deglaciation model (model L) will not result in a uniform rate of retreat throughout the last 20 ka (see Supporting Information).

The reason for testing these four deglacial scenarios is to determine the degree to which the differences in interpolation scheme influence predictions of RSL change, present-day uplift rates and geoid rates in Antarctica. The results will be used to place bounds on the uncertainty of GIA model predictions.

2.1.1 Pre-LGM ice build-up

Due to the viscoelastic properties of the mantle, surface load changes throughout the last glacial cycle combine to define the present-day GIA response, and the ice-loading model is therefore extended back to 122 ka BP; the middle of the Last Interglacial (LIG). We make the assumption that the configuration of the AIS during the LIG was the same as the present-day. While there is evidence to suggest that the eustatic volume of the AIS may have been at least 2.5 m smaller during this period (Kopp *et al.* 2009), sensitivity tests (not shown here) indicate that this will have a negligible impact upon predictions of present-day GIA observables.

In our ice build-up model it is assumed that the AIS grows to 50 per cent of its 20 ka BP extent by 100 ka BP with the final 50 per cent of growth occurring linearly between 100 and 30 ka BP. LGM conditions are then maintained for 10 ka before the initiation of deglaciation. This model of ice volume increase has been devel-

oped to mimic previous modelling attempts which were driven by climate forcing throughout the last glacial cycle (Ritz *et al.* 2001; Huybrechts 2002; Pollard & DeConto 2009); specific time slices were not reconstructed during ice build-up due to the absence of field constraints during this period.

Previous studies have shown that RSL predictions in former glaciated regions can differ by a factor of two when glacial build-up conditions are varied between a model which assumes isostatic equilibrium at the LGM and a model which incorporates a rapid glaciation phase (Mitrovica & Davis 1995). To assess the sensitivity of our Antarctic GIA model to pre-LGM ice-sheet changes additional scenarios of ice-sheet build-up, in which the timing of ice build-up and the duration of the LGM are altered, are tested (not shown here). The end-member case of isostatic equilibrium at the LGM is not considered since far-field sea-level data indicate that the AIS underwent a significant increase in ice volume between the LIG and the LGM. The experiments confirm that reasonable perturbations to the timing of ice build-up prior to the LGM have a negligible effect upon present-day uplift rates ($<0.5 \text{ mm yr}^{-1}$), RSL predictions (1–2 m during the period when data are available), and geoid rates ($<0.05 \text{ mm yr}^{-1}$) in relation to the accuracy of the existing data sets, and therefore we are justified in using the model described above in all experiments.

2.1.2 Far-field deglaciation model

RSL change and solid Earth deformation in Antarctica are influenced by both far-field and near-field changes in surface loading during the last glacial cycle. These GIA model outputs are calculated by solving the sea-level equation (Farrell & Clark 1976), which requires knowledge of the global history of ice loading. We use the existing ICE-5G v1.2 global deglaciation model (Peltier 2004; hereafter just ICE-5G), but replace the Antarctic component with the W12 ice-loading history, to create a new global ice-loading model which delivers a eustatic contribution of $\sim 128 \text{ m}$ to the ocean between 21 ka BP and the present day. This eustatic calculation includes contributions from ice grounded below the geoid (Milne *et al.* 1999).

The ICE-5G model contains an Antarctic component, which is equivalent to 17.3 m eustatic sea-level (ESL) change between the LGM and the present (Peltier 2004). Since the Antarctic deglaciation history of Whitehouse *et al.* (2012) only contains $\sim 8 \text{ m}$ ESL change between 20 ka BP and the present, the composite global deglaciation model that we have created will no longer fit the extensive RSL database to which the ICE-5G model is tuned. This composite model should therefore not be used to investigate far-field RSL change and it should not be used to ‘fingerprint’ the sources of ESL changes (Bassett *et al.* 2005). However, since near-field GIA is dominated by the response to ice-mass changes, our model is suitable both for investigating GIA in Antarctica and subtracting from GRACE observations made over Antarctica. We choose to use the ICE-5G model since it is the most coherent global model currently available, and it contains a relatively small Antarctic component, thus minimizing the issue of altering the total eustatic volume; this issue is further discussed in Section 4.1.2.

2.2 GIA modelling

The global ice-loading history described in Section 2.1 is input to a GIA model to solve the sea-level equation (Farrell & Clark 1976). This equation solves for solid Earth deformation and gravitationally

consistent perturbations to the shape of the geoid over time due to the global redistribution of internal and surface mass throughout the last glacial cycle. This mass redistribution is due to both ice and ocean loading. The change in the distance between the solid surface and the ocean surface (neglecting dynamic topography) across each time step defines the change in RSL. The GIA model accounts for shoreline migration, changes in loading due to the retreat of marine-grounded ice (Mitrovica & Milne 2003; Kendall *et al.* 2005), and rotational feedback (Milne & Mitrovica 1998; Mitrovica *et al.* 2005). Inputs to the GIA model are ice-loading history and Earth rheology and density structure. Outputs of the GIA model include predictions of RSL change over time and present-day solid Earth uplift rates.

2.2.1 Topography

At all times since the LGM large portions of the AIS have been marine-grounded, that is, grounded below sea level. Within the GIA model, W12 ice thicknesses and palaeotopography are used to determine where ice is grounded, and where it is floating at each time step. Palaeotopography $T(x, t)$ at location x and time t is calculated to be the difference between present-day topography $T(x, 0)$ and RSL change $\Delta RSL(x, t)$

$$T(x, t) = T(x, 0) - \Delta RSL(x, t). \quad (1)$$

The loading history that drives the GIA model is dependent upon the change in the mass of ice or water at each point, across each time step. Care is taken to record the transition from grounded to floating ice at the margin of the ice sheet to ensure that the change in loading between time steps is correctly defined.

ALBMAP is used to define present-day bedrock topography south of 55°S (Le Brocq *et al.* 2010). The ALBMAP data set is taken from the same data set as the present-day ice thickness distribution used in W12 (Le Brocq *et al.* 2010), therefore the distribution of floating and grounded ice at the present day will be correctly determined by the algorithm within the GIA model. North of 55°S, the ETOPO2v2 (2006) data set is used because it is the recommended data set for use with ICE-5G v1.2. Across Greenland, ETOPO2v2 depicts ‘ice surface’ instead of bedrock elevation, and therefore the algorithm, which determines whether ice is floating or grounded may fail in marine-grounded areas. However, due to the small area of Greenland that is currently marine-grounded, any errors incurred will have a negligible effect upon GIA predictions in Antarctica.

2.2.2 Earth model

Earth rheology and density structure govern the solid Earth response to surface-load changes over time. The earth model that we use is a compressible, spherically symmetric, self-gravitating Maxwell viscoelastic body. The elastic and density structure are derived from PREM (Dziewonski & Anderson 1981), the lithosphere is depicted by a layer of very high viscosity, and the upper and lower mantle are defined to be uniform viscosity layers which extend to the 660 km discontinuity and the core–mantle boundary (2900 km), respectively.

The rheological parameters of most relevance to GIA predictions are lithospheric thickness and the viscosity of the lower and upper mantle; these are not yet well constrained by observations in Antarctica. They are therefore treated as unknown within bounds, and the combination of rheological parameters that gives the best fit to observations of RSL change around Antarctica is sought. 297

earth models are investigated in which the lithospheric thickness can take the value 71 km, 96 km or 120 km, the upper mantle viscosity can be any one of [0.05, 0.08, 0.1, 0.2, 0.3, 0.5, 0.8, 1.0, 2.0, 3.0, 5.0] $\times 10^{21}$ Pa s, and the lower mantle viscosity can be any one of [1, 2, 3, 5, 8, 10, 20, 30, 50] $\times 10^{21}$ Pa s. The far-field ICE-5G deglaciation history is tuned to fit global constraints when used in conjunction with the VM2 viscosity model (Peltier 2004). We accept that our composite ice-loading history will not necessarily fit these global constraints due to the use of a range of radially-varying earth models in an attempt to fit the near-field Antarctic constraints, but note that the impact of using earth models other than VM2 in conjunction with far-field loading has a negligible impact upon GIA in Antarctica. For the full range of earth models, uplift rates within Antarctica due to far-field ice-loading are perturbed from VM2 values by <0.5 mm yr⁻¹.

3 DATA

3.1 Relative sea-level constraints

GIA model output is compared with RSL data from 14 sites around the Antarctic coast, and marine limit (ML) observations from six additional sites (see Fig. 1). The data set that we use is similar to, but updated from, that documented within Bassett *et al.* (2007). Our data set includes additional data from the South Shetland Islands (Watcham *et al.* 2011; Simms *et al.* 2011, and references therein), and new data from James Ross Island (Hjort *et al.* 1997), Beak Island (Roberts *et al.* 2011), Ablation Point (Roberts *et al.* 2009), and Pine Island Bay (Johnson *et al.* 2008) in West Antarctica, and the Windmill (Goodwin 1993) and Rauer (Berg *et al.* 2010) islands in East Antarctica (Fig. 1). Undated MLs from Oates Land, George V Land, Eastern Wilkes Land, Budd Coast, Knox Coast and Beaver Lake in East Antarctica provide additional constraints on the ice-loading history (Adamson *et al.* 1997; Goodwin & Zweck 2000), and an undated freshwater-marine transition at 54 m below sea level further documents Holocene RSL change at Beaver Lake (Wagner *et al.* 2007).

Our data set includes records of lake isolation events, raised beach deposits, and exposure ages from an unnamed emergent island. Issues relating to the dating of Antarctic material are discussed elsewhere (Björck *et al.* 1991) and we refer the reader to the original references listed above for further information on the dating techniques used at each site. The indicative meaning of each RSL datum has been quantified, and this is used to determine the degree of fit between the observations and the predictions output from the GIA model. It is assumed that data from locations within a 20 km radius may be combined to form a single RSL curve. Where the data come from a wider area, sensitivity tests are carried out to determine whether the data may be combined, and in the case of the two South Shetland Islands sites and the three Prydz Bay sites (see Fig. 1), caution has been applied and separate RSL predictions are generated for each site.

3.2 Observations of present-day uplift rates

GIA model output is also compared with a recently compiled Antarctic-wide GPS data set (Thomas *et al.* 2011). Details of the GPS sites are listed in Table S2. We note that errors are incurred in making this comparison, firstly because GIA model rates and the GPS-derived uplift rates are in different reference frames [centre of mass of solid Earth and entire Earth system, respectively;

Table 1. GIA Experiments. Italicized entries highlight the difference between Experiments 2, 3 and 4 and the control Experiment 1. Details of the 16 ice-sheet reconstructions used in Experiment 3 are given in Table S1. S = stepped deglaciation model; S2 = stepped deglaciation model with rapid melt across meltwater pulse 1A; L = linear deglaciation model; L2 = linear deglaciation model with no melt after 2 ka BP. The parameter space for the earth models is given in Section 2.2.2 of the text. The optimum earth model is that which minimizes the misfit to the RSL data, and the optimum range contains earth models that lie within the 95 per cent confidence limit of the RSL analysis (see text). All experiments are run using the pre-LGM ice build-up model described in Section 2.1.1.

Experiment	Deglaciation model	Style of deglaciation	earth model	Notes
1	W12 deglaciation model	S	All earth models	Use RSL and GPS data to determine best earth model
2	W12 deglaciation model	<i>S, S2, L, L2</i>	<i>Optimum earth model</i>	Sensitivity of GIA predictions to the rate/timing of deglaciation
3	<i>16 deglaciation models^a</i>	S	<i>Optimum range of earth models</i>	Sensitivity of GIA predictions to uncertainties in ice-load history
4	<i>'adjusted' W12a deglaciation model</i>	S	<i>Optimum range of earth models</i>	Seek to fit GPS observations of uplift in the Antarctic Peninsula

^aSee Table S1.

see Kleemann & Martinec (2011)], and secondly due to the effect of present-day surface mass transport upon the motion of the centre of mass, a process which is not included in our GIA model. The combined magnitude of these differences is estimated to be $<0.5 \text{ mm yr}^{-1}$ (e.g. Kleemann & Martinec 2011; Rietbroek *et al.* in press).

Apart from sites in the northern Antarctic Peninsula, we use the GPS uplift rates of Thomas *et al.* (2011) after applying their model of elastic rebound (mass flux version—see auxiliary material of Thomas *et al.* 2011). As noted by Thomas *et al.* (2011), however, this model does not satisfactorily account for the sizeable rebound which has been taking place in the northern Antarctic Peninsula since 2002 due to the break-up of the Larsen B ice shelf (Rignot *et al.* 2004). At present, the ratio of elastic to viscoelastic deformation in response to this break-up is poorly understood (Ivins *et al.* 2011), therefore, we do not attempt to model this response, and instead follow the suggestion of Thomas *et al.* (2011) in using pre-2002 velocities as an upper bound on GIA-related uplift in this region. Apart from where noted we do not tune the GIA model to fit the GPS uplift data.

4 RESULTS

Four groups of experiments are carried out (see Table 1): using the W12 deglaciation model, the GIA model is calibrated by seeking the earth model that provides the best fit to the RSL data. This model is tested by comparing uplift rate predictions to elastic-corrected GPS data, and the sensitivity of the model to uncertainties in the earth model and ice-loading history is quantified. Finally, an adjustment is made to the W12 deglaciation history in the Antarctic Peninsula to investigate an improved fit to the GPS data.

4.1 Sensitivity to earth model (Experiment 1)

4.1.1 Comparison to RSL data

The W12 deglaciation model is interpolated in time using the stepped method (Model S, see Section 2.1), and combined with the full suite of earth models (see Section 2.2.2) to form the input for 297 runs of the GIA model. In Fig. 3 the range of RSL predictions at each site for all 297 earth models is covered by the grey shaded region. A narrow range of predictions, for example, for Sôya or Fildes Peninsula, indicates a weak sensitivity to the choice of earth model, while a wider range of predictions indicates a stronger sensitivity to the choice of earth model. The available

RSL data are also plotted in Fig. 3, and the goodness of fit for each earth model is quantified by calculating the χ^2 value for each site j :

$$\chi_j^2 = \frac{1}{n_j} \sum_{i=1}^{n_j} \left(\frac{y_i^p - y_i^o}{\sigma_i} \right)^2. \quad (2)$$

n_j is the number of RSL observations at site j , y_i^p and y_i^o are the predicted and observed RSL values, respectively, for data point i , and σ_i is the normalized observational error at that data point:

$$\sigma_i = \frac{1}{\sqrt{2}} \sqrt{\left(\frac{t_i}{t_{\max}} \right)^2 + \left(\frac{h_i}{h_{\max}} \right)^2}. \quad (3)$$

t_i is the dating error for data point i , t_{\max} is the largest dating error, h_i is the elevation error on the RSL measurement at data point i , and h_{\max} is the largest elevation error. If the RSL prediction passes above or below a limiting, that is, minimum or maximum, data point then a good fit is achieved and the χ^2 statistic is assigned a value of 1 in this case. In addition, combined χ^2 values are calculated for (i) all sites, (ii) just West Antarctic sites, and (iii) just East Antarctic sites (Fig. 4).

There is no single earth model, or small subset of earth models, that simultaneously fits the data well at all sites. However, a good fit can be achieved at each site by choosing a site-specific best-fit earth model (Fig. 3, black lines). In Fig. 4, χ^2 values are plotted for the full range of earth models to explore the sensitivity of the data to the different parameters of the Earth viscosity model. For each grouping of sites (columns 1, 2 and 3, Fig. 4) the 95 per cent confidence limit is plotted as a dashed line. We note that the inclusion of data from Marguerite Bay increases the χ^2 values, and biases the choice of earth model, when the earth model that best fits the RSL data is sought. The reason for this is that there is likely too much ice in the LGM ice-sheet reconstruction in Marguerite Bay (Whitehouse *et al.* 2012), and therefore extreme earth models are sought in an attempt to fit the data. RSL data from Marguerite Bay are therefore not included in the analysis presented in Fig. 4. We do not discuss this site further here, but return to the implications of the misfit in Section 5.

The χ^2 values for the full RSL data set (Fig. 4, first column) exhibit a weak dependence upon lithospheric thickness and lower mantle viscosity and a strong dependence upon upper mantle viscosity, with a preference for viscosity values in the range $\sim 0.5\text{--}2.0 \times 10^{21} \text{ Pa s}$. The best-fitting model (red star) has a lithospheric thickness of 120 km, an upper mantle viscosity of $1 \times 10^{21} \text{ Pa s}$, and a lower mantle viscosity of $10 \times 10^{21} \text{ Pa s}$. We refer to this earth model as the optimum earth model for the RSL data.

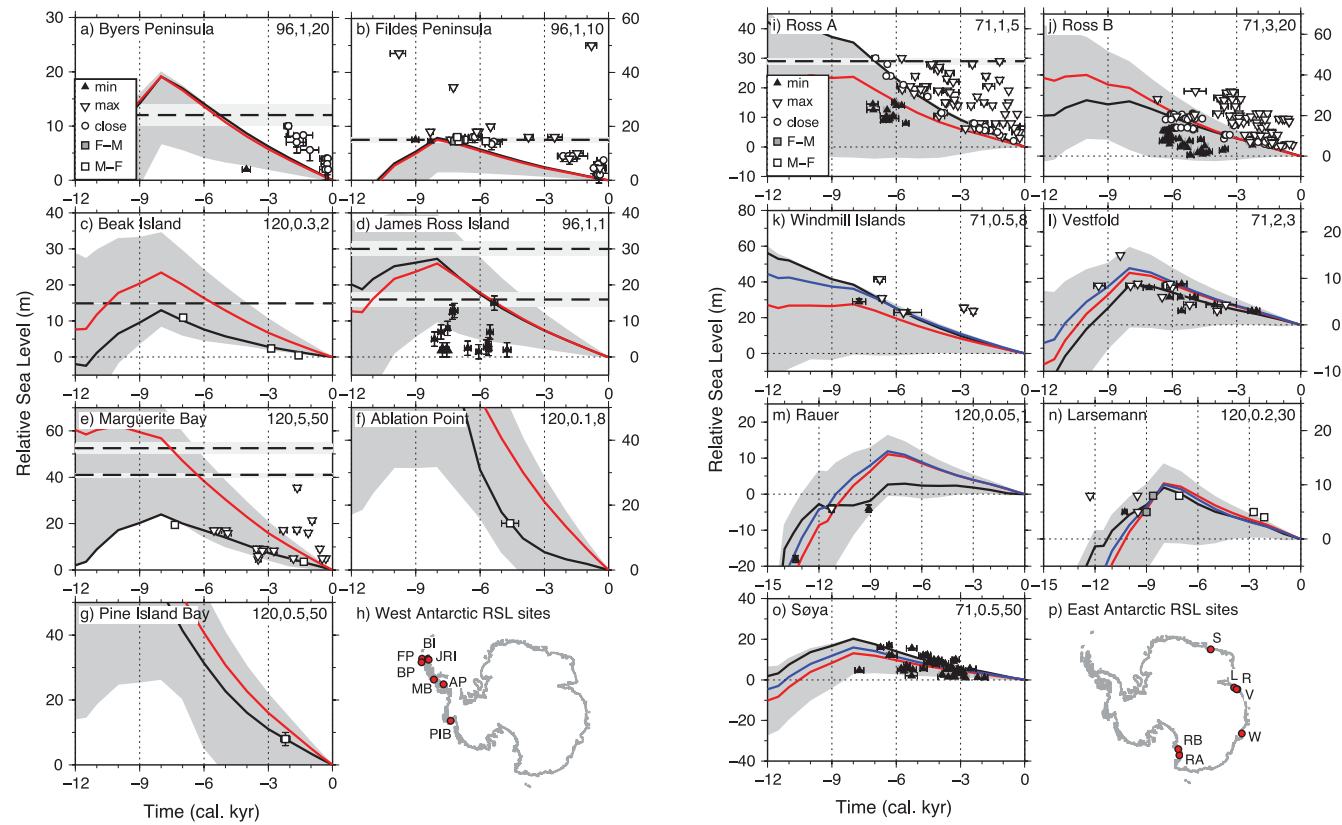


Figure 3. RSL data and predictions at 14 sites around Antarctica. The W12 ice-loading history with the stepped time interpolation is used for all predictions. In each plot the grey shaded region depicts the range of predictions at that site for all 297 earth models considered. Note the different vertical scale used in each plot. The curve for the best-fitting earth model at each site is plotted as a black line, and labelled in the top right of each plot according to the following convention: lithospheric thickness (km), upper mantle viscosity ($\times 10^{21}$ Pa s), lower mantle viscosity ($\times 10^{21}$ Pa s). The curve calculated using the earth model that best fits all the RSL data is shown in red, and the curve calculated using the earth model that best fits the East Antarctic data is shown in blue (3k–o). The earth model that best fits the West Antarctic data is identical to that which fits the full Antarctic data set. Where available, the observed local marine limit (ML) is plotted as a horizontal dashed black line with the error shown in pale grey (two MLs are recorded at James Ross Island and Marguerite Bay). The RSL data are plotted on top of the predictions according to the following convention: Upward-pointing black triangles are minimum data; downward-pointing white triangles are maximum data. The RSL curve should pass above/below these data, respectively. Data that are found close to sea level, for example, material within raised beaches, are plotted with an open circle. Isolation basin data that represent a transition from freshwater to marine conditions are plotted as a grey square, and data that represent a transition from marine to freshwater are plotted as a white square. The RSL curve should pass through these data as a rising/falling line, respectively. The locations of the RSL sites are plotted in Figs 3(h) and (p).

The relatively high χ^2 values within the 95 percent confidence limit of the first column of Fig. 4 reflect the poor fit to the RSL data at several sites, including Beak Island, Ablation Point, Vestfold Hills, Larsemann Hills, and Søya, when the optimum earth model is combined with the W12 deglaciation history within the GIA model (Fig. 3, red lines). The reason for the poor fit may relate to errors in the ice-loading history, the quality of the RSL data, or the fact that lateral variations in Earth structure across Antarctica do not permit all the data to be accurately modelled using a single earth model. With this in mind, the data are divided and the best-fitting earth model for the West (Figs 3a–j) and East (Figs 3k–o) Antarctic sites is sought separately. The two Ross Sea sites [Terra Nova Bay (Ross A) and Southern Victoria Land (Ross B)] are situated on the geological boundary between East and West Antarctica, but due to their proximity to the West Antarctic Rift System, and the presence of low seismic velocities beneath these sites (Morelli & Danesi 2004), we define them to lie within West Antarctica.

The high χ^2 values for the West Antarctic sites (Fig. 4, middle column) indicate that there is no single earth model that can fit the RSL data at all these sites. This is also apparent from the wide range of preferred site-specific earth models in Figs 3(a)–(j). The

distribution of χ^2 values for these sites implies a dependence upon both upper and lower mantle viscosity values, with a preference for a relatively high viscosity in both cases. The best-fitting earth model for the West Antarctic sites (green star) has a lithospheric thickness of 120 km, an upper mantle viscosity of 1×10^{21} Pa s, and a lower mantle viscosity of 10×10^{21} Pa s; this is the same as the optimum earth model for the full data set.

The lowest χ^2 values are calculated for the East Antarctic data (right column, Fig. 4). χ^2 values for these sites are strongly dependent upon the upper mantle viscosity, but there is almost no dependence upon lower mantle viscosity, and χ^2 values for all lithospheric thicknesses are almost identical. The best-fitting earth model for the East Antarctic sites (blue star) has a lithospheric thickness of 71 km, an upper mantle viscosity of 1×10^{21} Pa s, and a lower mantle viscosity of 2×10^{21} Pa s. RSL predictions for this model are plotted in blue in Figs 3(k)–(o).

4.1.2 Comparison to marine limit data

In Antarctica a ML may be formed in one of two situations; during an RSL highstand or immediately following the retreat of

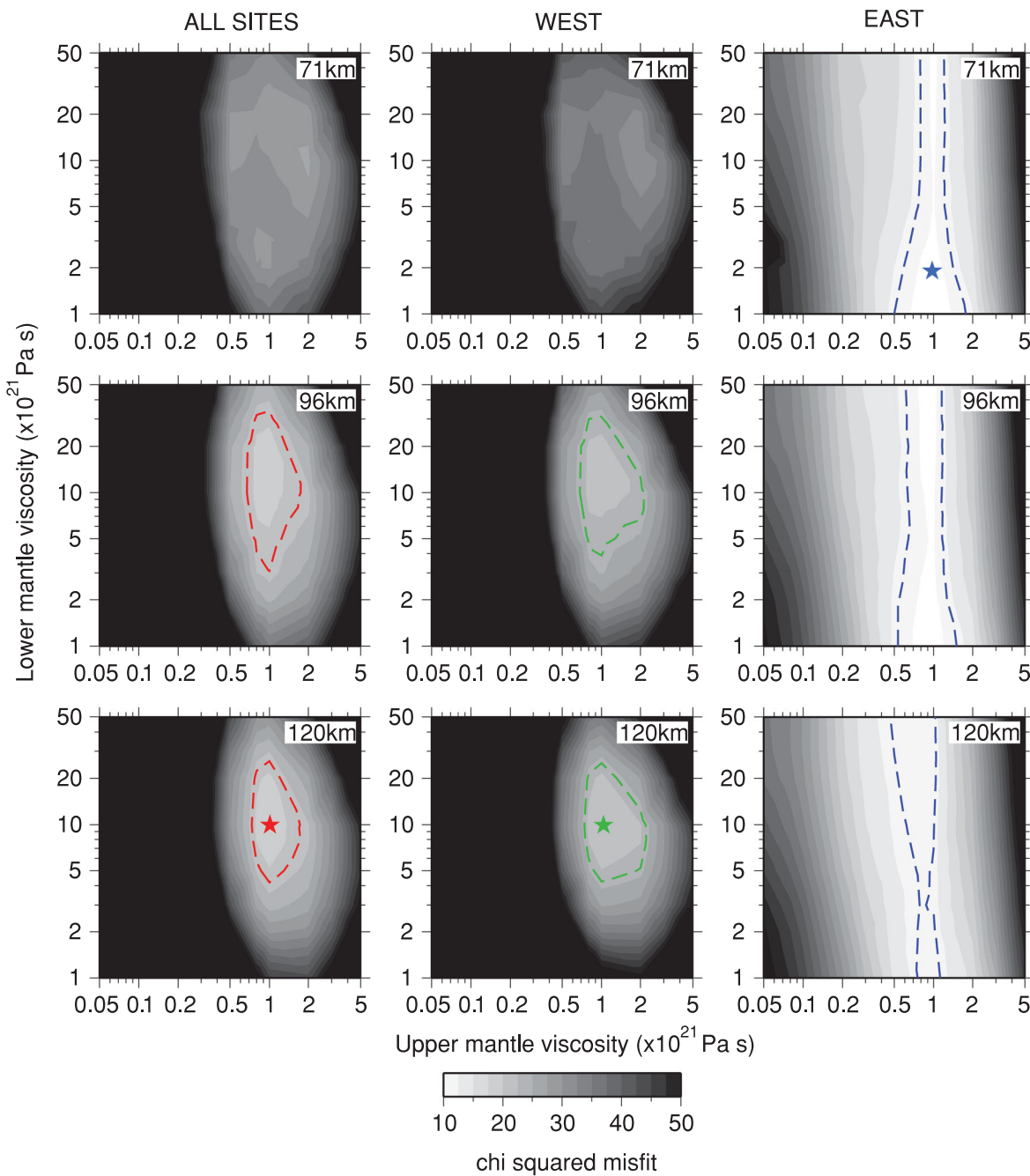


Figure 4. χ^2 log–log plots for the RSL data. The W12 ice-loading history with the stepped time interpolation is used to calculate RSL predictions at all sites, for all earth models. In each plot χ^2 values are given for the same ranges of upper and lower mantle viscosity. In the first row the lithospheric thickness is 71 km, in the second it is 96 km, and in the third it is 120 km. In the first column, data at all the RSL sites except Marguerite Bay are used, in the second column only data from sites in West Antarctica (excluding Marguerite Bay) are used (see main text), and in the third column only data from sites in East Antarctica are used. For each group of sites (column) the 95 per cent confidence limit is plotted as a dashed line, and the best model is identified by a star.

Downloaded from https://academic.oup.com/gji/article/190/3/1464/570434 by Victoria University user on 10 December 2021

marine grounded ice to an onshore position. The complex interplay of ocean, solid Earth, and ice processes required to form a ML (Andrews 1970) means that they may be found at a range of heights around the coast of Antarctica. Many of the MLs are undated, and we make the assumption that those discussed here have been formed since the LGM. By analysing the timing of ice retreat and the range of RSL predictions at each ML site (Fig. 3) it is determined whether there is an ice–earth model combination that supports the formation

of each ML. A ML formed as a result of ice retreat should cut the falling limb of a RSL curve at the time of ice retreat, while a ML formed during a highstand should just skim the top of a RSL curve (Fig. 3).

The MLs at Byers Peninsula (Björck *et al.* 1996), James Ross Island (Hjort *et al.* 1997), Marguerite Bay (Bentley *et al.* 2005) and Terra Nova Bay (Ross A; Baroni & Hall 2004) are likely to have been formed at the time of local ice retreat. Using the W12

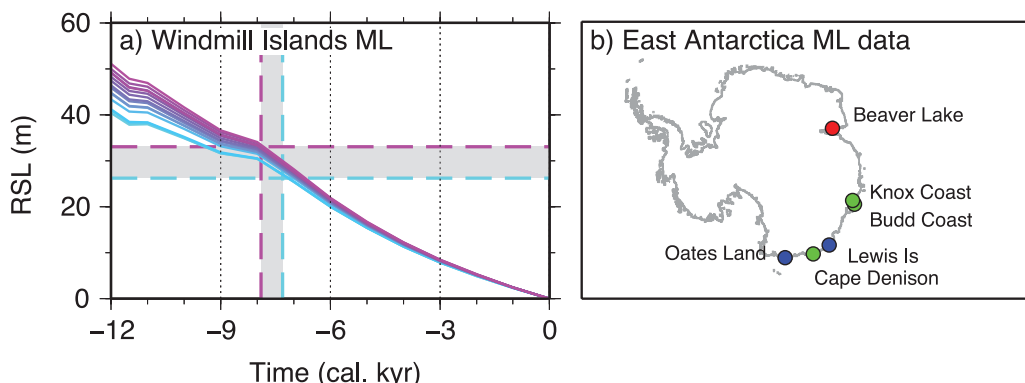


Figure 5. Observations and predictions relating to ML data in Antarctica. (a) RSL predictions for 14 sites in the Windmill Islands (western Budd Coast) at which the ML is recorded. The curves are plotted in different colours to distinguish between the sites: the northernmost site is plotted in cyan, and the southernmost site is plotted in magenta, with intermediate sites following the cyan-magenta colour scale according to latitude. The range of observed MLs is plotted as a horizontal grey bar. The lower limit corresponds to the ML at the northernmost site (cyan dashed line), and the upper limit corresponds to the ML at the southernmost site (magenta dashed line). The times at which the RSL predictions for the northern (cyan dashed line) and southernmost (magenta dashed line) sites cross the relevant observed MLs are marked as vertical lines. A vertical grey box is drawn to highlight the period of deglaciation, assuming the MLs formed as the ice retreated. (b) A circle is plotted at the location of six additional ML observations. The colour of the circle denotes whether the predicted RSL curves for that site lie completely below the ML (blue), pass above the ML (red), or cross the height of the local ML (green). (The circles at Knox and Budd Coasts are both green.)

deglaciation model it is possible to find an earth model that replicates the formation of each of these MLs (Figs 3a, d, e and i). The timing of deglaciation at Fildes Peninsula (Watcham *et al.* 2011) and Beak Island (Roberts *et al.* 2011) indicates that the MLs at these sites were formed during RSL highstands. Once again, the deglaciation model is able to reproduce the formation of these MLs for some choice of earth model (Figs 3b and c).

MLs in the Windmill Islands display a north–south trend, with higher MLs found to the south (Goodwin 1993). The observations are undated, but an RSL curve is calculated for each site, for a mid-range earth model, and we note that our predictions display the same north–south trend (Fig. 5a). Making the assumption that the MLs were formed due to the retreat of the ice sheet, the intersection between the RSL prediction and the observed ML at each site is used to estimate the timing of deglaciation. In close agreement with Goodwin (1993), we estimate deglaciation to have taken place between 8 and 7 ka BP, with the southern sites deglaciating first, in accordance with ice retreat towards Law Dome.

Additional ML observations have been documented at six sites in East Antarctica (Fig. 5b; Goodwin & Zweck 2000, and references therein). At two of these sites, Oates Land and Lewis Island, none of the earth models is able to reproduce a RSL highstand at the height of the observed MLs (29 and 30 m, respectively), with the best models falling short by just ~ 2 m. At three of the sites, Cape Denison, Knox Coast and Budd Coast, the range of RSL predictions encompasses the ML elevations, and therefore our GIA model is able to replicate the formation of these features.

At Beaver Lake, a subset of the predictions (not shown) pass through the undated freshwater-marine transition at 54 m below sea level (Wagner *et al.* 2007) around 15 ka BP, implying early deglaciation at this site. In addition, geomorphic evidence indicates that RSL has not been above present at this site since deglaciation (Adamson *et al.* 1997). Using the W12 deglacial history, our model predicts a minimum Holocene highstand of ~ 2 m at Beaver Lake, indicating that the ice-loading history may need revising downward there.

Alternatively, we note that the use of a different eustatic curve, that is, far-field loading history, may rectify the misfit, both at this

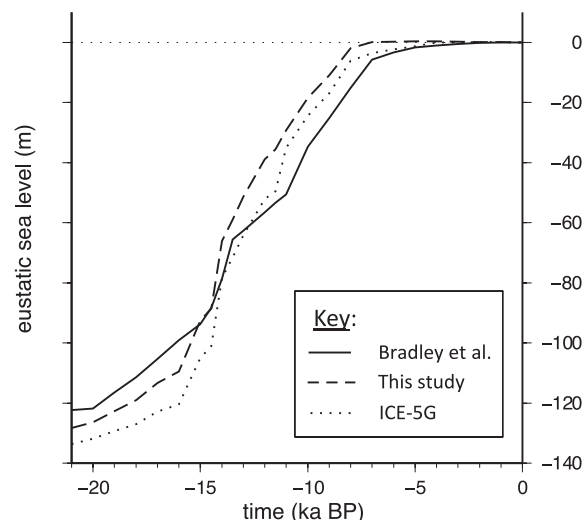


Figure 6. Eustatic curves for the Bradley *et al.* model (2008) (solid line), this study (dashed line), and ICE-5G (dotted line).

site and others. By substituting the ICE-5G v1.2 Antarctic component with the W12 deglaciation model, we alter the time-dependent global volume of grounded ice, or equivalently, the eustatic component of the ice-loading history. To assess the implications of the resulting errors in the eustatic component of our composite model, we compare our eustatic component to the eustatic component of the original ICE-5G model (Peltier 2004) and one other eustatic model (Bradley *et al.* 2008; see Fig. 6). Differences are up to ~ 20 m during the early period of deglaciation, but during the period when RSL data are available in Antarctica (Holocene, and mainly the mid-to-late Holocene), differences are < 10 m, decreasing to zero during the last few thousand years.

We do not seek to carry out an assessment of which of the two eustatic models considered is more accurate, but simply use this comparison to highlight the possibility that RSL predictions in areas which do not undergo substantial solid Earth deformation could be

shifted significantly if a more accurate eustatic history was adopted. The site-specific viscosity inferences at such sites (Fig. 3) will be biased. However, at the majority of our RSL sites, the perturbation to the predictions is small in comparison with the total predicted RSL change and so this bias is likely to be minor. The influence of the perturbation on the regional viscosity inferences will also be small since the model predictions lie both above and below the data at an (approximately) equal number of sites (Fig. 3). Finally, at sites like Beaver Lake the adoption of an alternative eustatic history, such as that of Bradley *et al.* (2008), would decrease the magnitude of the highstand by 1–2 m, thus accounting for the small misfit which persists when we use the ICE-5G/W12 composite history. A detailed discussion of the model fit to all the RSL data is included in the Supporting Information.

4.1.3 Comparison to GPS uplift rates

The earth models that lie within the 95 per cent confidence limit of the RSL data analysis (Fig. 4, column 1) are assumed to provide bounds on realistic earth model parameters. The robustness of this result is tested in Section 4.2.2, but first the sensitivity of uplift rates to variations in earth model parameters is investigated.

Using the W12 deglaciation history, the earth model that minimizes the misfit to the elastic-corrected GPS-observed uplift rates (Thomas *et al.* 2011) is very similar to that which minimizes the misfit to the RSL data, the only difference being that the GPS data prefer an earth model with a slightly higher upper mantle viscosity of 2×10^{21} Pa s. This agreement in preferred earth models gives us confidence that our modelling is robust. The maximum range of uplift rates produced by the 17 earth models that lie within the 95 per cent confidence limit of the RSL data analysis is ~ 2.7 mm yr $^{-1}$ (Fig. 7a), and occurs in regions which also experience the greatest absolute present-day uplift rates. In Fig. 7(b) predicted and observed (elastic-

corrected) present-day uplift rates are plotted at each of the 35 GPS sites (coloured dots), where the predicted rates are calculated using the W12 deglaciation history and the optimum earth model from the RSL analysis (see also Table S2). The spread due to model uncertainty (horizontal error bars, Fig. 7b) is of the same order of magnitude as the GPS error (vertical error bars, Fig. 7b), and, considering all sites, the predicted uplift rates are biased high compared with the observed uplift rates (weighted mean bias = 1.8 mm yr $^{-1}$; weights are taken to be the GPS uncertainty at each site, as given in Table S2).

The Weighted Root-Mean-Square (WRMS) error is used to assess the degree of fit between the GIA model output and elastic-corrected GPS observations of GIA-driven uplift:

$$\text{WRMS} = \sqrt{\frac{\sum_i (o_i - p_i)^2 w_i}{\sum_i w_i}}. \quad (4)$$

o_i and p_i are observed and predicted uplift rates, respectively, and w_i is the weighting for each datum. When the output from a single GIA model is being tested, the weighting is based on the GPS uncertainty (σ_i^{GPS}) at each site: $w_i = \frac{1}{(\sigma_i^{\text{GPS}})^2}$. However, when we analyse the fit of a range of predictions to the GPS data, WRMS values also account for ‘model uncertainties’:

$$w_i^{\text{W12}} = \frac{1}{(\sigma_i^{\text{GPS}})^2 + (\sigma_i^{\text{GIA}})^2}, \quad (5)$$

where σ_i^{GPS} is the 1-sigma uncertainty on the GPS observation at site i , and σ_i^{GIA} is the range of predicted uplift rates at that site. Considering the output when the W12 deglaciation model is combined with each of the earth models that lie within the 95 per cent confidence limit of the RSL data analysis, the WRMS error is 2.7 mm yr $^{-1}$ (Fig. 7b).

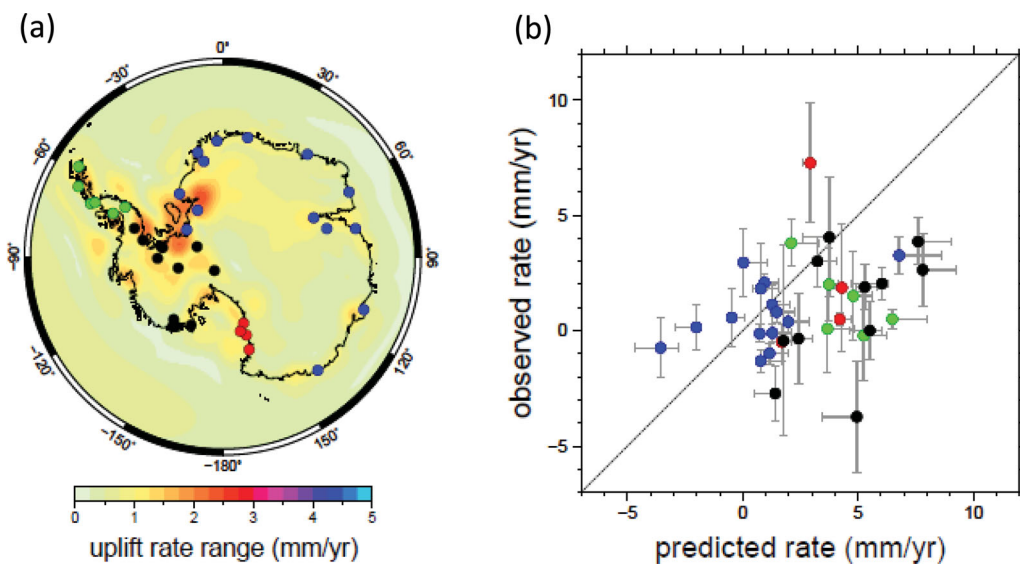


Figure 7. Sensitivity of present-day uplift rates to variation across 17 earth models. (a) Magnitude of the range of present-day uplift rates for all earth models that have a χ^2 value within the 95 per cent confidence limit when we consider all RSL sites (see Fig. 4, first column). The W12 ice-loading history with model S is used for all predictions. The locations of the 35 GPS sites listed in Table S2 are plotted according to the following code: Ross Sea (red), Antarctic Peninsula (green), East Antarctica (blue), West Antarctica (black). (b) Observed (elastic-corrected) vs. predicted present-day uplift rates at the 35 GPS sites. Predicted rates are for the best ice-earth model combination; colours indicate the region the data/predictions relate to (as shown in Fig. 7a). Vertical error bars are 1-sigma uncertainties for the GPS data, horizontal error bars are defined using the range of predicted rates for earth models that have a χ^2 value within the 95 per cent confidence limit (Fig. 4, first column). The horizontal error bars may be asymmetric.

4.2 Sensitivity to ice-loading history

4.2.1 Rate and timing of deglaciation (Experiment 2)

Having considered GIA model sensitivity to the choice of earth model, sensitivity to the ice-loading history is now investigated. In Fig. 8 differences in predicted present-day uplift rates between the four interpolation methods described in Section 2.1 are plotted. In all cases, the W12 deglaciation model is interpolated, and the GIA model is run using the optimum earth model of Experiment 1. Model S and model L2 only differ prior to 5 ka BP (Fig. 2). The maximum difference in predicted present-day uplift rates between these two models is $\sim 0.5 \text{ mm yr}^{-1}$ (Fig. 8a), indicating that small perturbations to the timing and rate of deglaciation prior to 5 ka BP have a negligible effect upon present-day uplift rates. Model S2, which is the same as model S except that it includes rapid retreat between 14.5 and 14 ka BP (the timing of meltwater pulse 1A), also results in predictions that are similar to those for model L2 (Fig. 8b).

This is due to the relatively small eustatic contribution in the W12 model between 15 and 10 ka BP.

Due to the similarity of predicted present-day uplift rates for models S and L2, Figs 8(c) and (d) are almost identical. The greater magnitude of the signal in these plots (peaking at $\sim 2.4 \text{ mm yr}^{-1}$) indicates that ice-load changes during the last 5 ka BP have a measurable effect upon present-day deformation rates. The stepped model (model S) is used in Experiments 1, 3 and 4 because it most closely replicates the retreat history described by the geological data, however, differences between the two most likely models, S and L2, are incorporated into our assessment of the uncertainties in our new GIA model (see Section 5).

The effect of variations in the rate of deglaciation upon predictions of RSL change is also investigated. RSL predictions for all four models differ by $<5 \text{ m}$ during the period when data are currently available in Antarctica (not shown). The magnitude of the vertical and temporal error bars on the RSL data mean that this data set is unable to distinguish between the four interpolation models

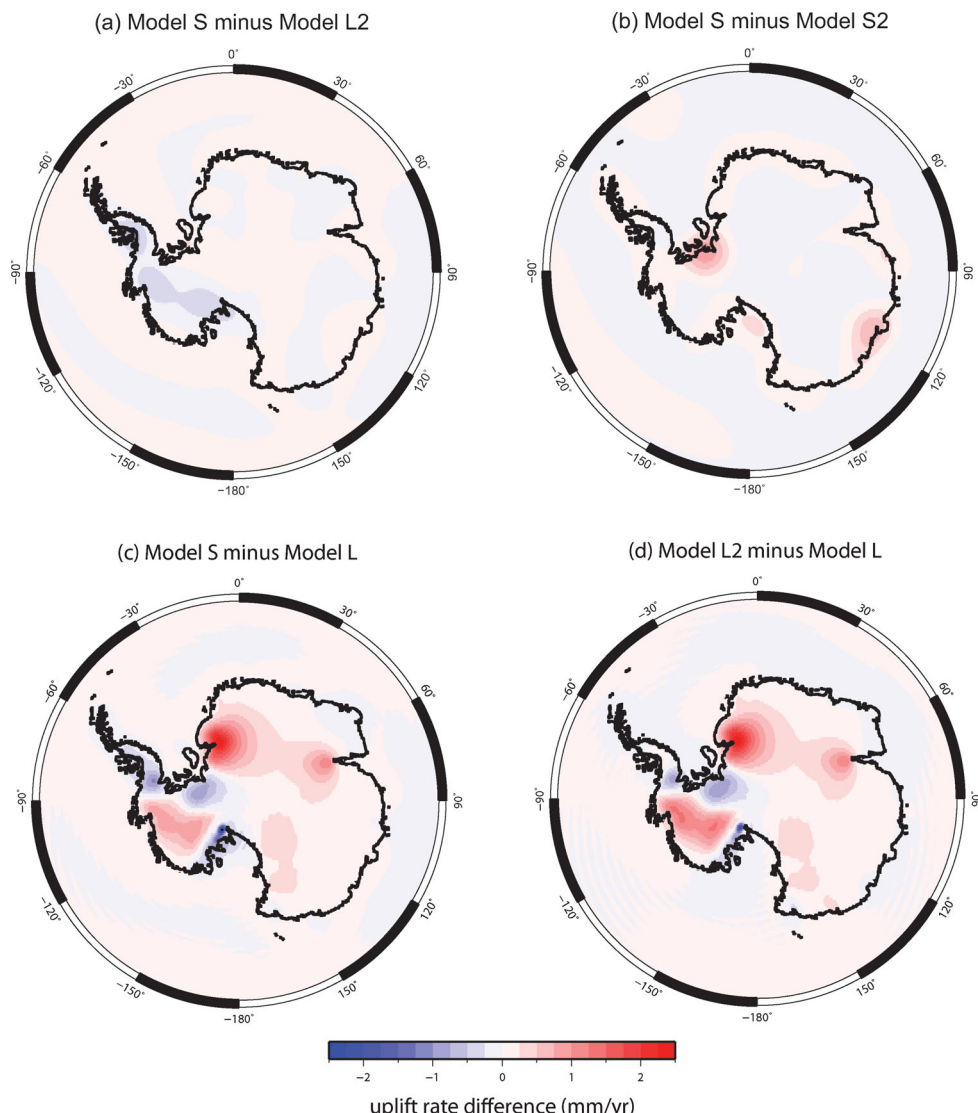


Figure 8. Sensitivity of present-day uplift rates to the rate and timing of deglaciation illustrated by differencing predictions for the four deglaciation scenarios. (a) Uplift rates for model S minus those for model L2. (b) Uplift rates for model S minus those for model S2. (c) Uplift rates for model S minus those for model L. (d) Uplift rates for model L2 minus those for model L. The optimum earth model (see text) and the W12 deglaciation model are used in all cases.

and the use of a different interpolation method is unlikely to alter the choice of optimum earth model.

4.2.2 Uncertainty in deglaciation history (Experiment 3)

Whitehouse *et al.* (2012) provide an estimate of the uncertainty in ice thickness change since the LGM due to incomplete knowledge of the climate history, geothermal heat flux distribution, rheological properties and relative sea-level forcing for Antarctica. In total, 16 model variants were produced (see Table S1), and these are used to investigate the sensitivity of GIA model output to uncertainty in the ice-loading history. The preferred deglaciation history is defined by the italicized models in Table S1 and is identical to the model that we refer to as W12. In all cases the stepped model (model S) is used to interpolate between 5 ka time slices, and, initially, the optimum earth model of Experiment 1 is used.

In Fig. 9(a) the magnitude of the range of predicted present-day uplift rates for the 16 deglaciation models is plotted. The maximum range is $\sim 2.1 \text{ mm yr}^{-1}$, and corresponds to locations where the ice sheet reconstruction displays the greatest uncertainty (Whitehouse *et al.* 2012). Fig. 9(b) compares the elastic-corrected GPS uplift rates (Thomas *et al.* 2011) with the predicted present-day uplift rates at the 35 GPS sites. The horizontal error bars, which are the same magnitude as the vertical GPS errors, represent the range of predicted uplift rates for the 16 deglaciation models.

Predicted LGM ice thicknesses vary by several 100 m in poorly constrained regions of the ice sheet reconstruction (Whitehouse *et al.* 2012), but over the full deglacial period these differences only result in present-day uplift-rate discrepancies of a few millimetres per year. To first order, the 16 deglaciation models used in this sensitivity test are very similar since they have been developed using the same grounding line extents and basal sliding parameters (Whitehouse *et al.* 2012). Therefore, in our experiments, we find that earth model and ice-history uncertainties contribute equally to the error budget (compare Figs 7 and 9). When the two sensitivity tests are combined, that is, both the deglaciation model and earth model are varied simultaneously (within the 95 per cent confidence limits of the RSL analysis), predicted uplift rates may vary by up to $\sim 4 \text{ mm yr}^{-1}$ in regions of maximum uplift, due to uncertainties in the GIA model inputs.

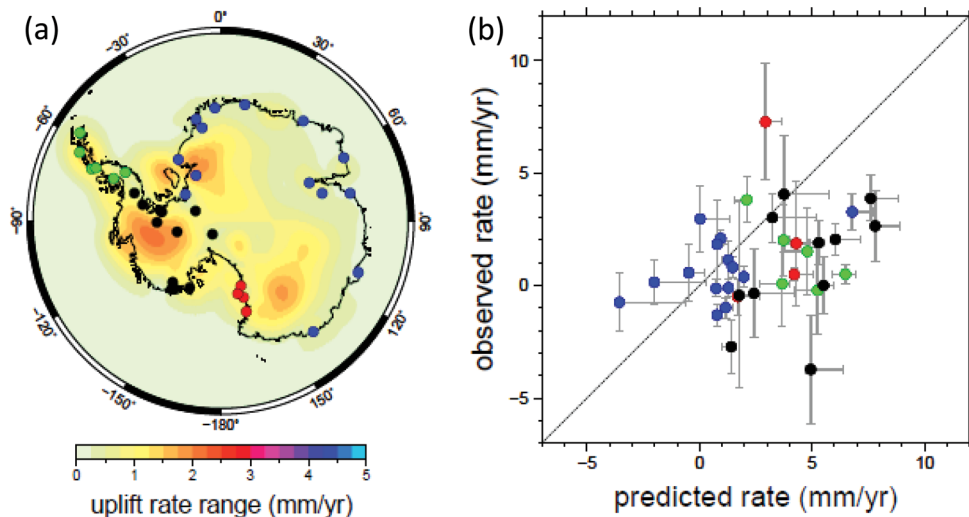


Figure 9. Sensitivity of present-day uplift rates to uncertainties in the ice-loading history. (a) Magnitude of the range of present-day uplift rates for the 16 deglaciation models of Experiment 3. The optimum earth model is used in all cases (see text). The locations of the 35 GPS sites are plotted as for Fig. 7. (b) Observed (elastic-corrected) vs. predicted present-day uplift rates at the 35 GPS sites. This figure is identical to Fig. 7(b) except that the horizontal error bars relate to the range of predicted rates for all 16 ice-loading models. The horizontal error bars may be asymmetric.

We note that this range may be biased because the range of earth models within the 95 per cent confidence limits of the RSL analysis were derived using a single deglaciation model (W12). This possibility is investigated by seeking the best-fit earth model (in terms of fitting the RSL data) for each of the 16 deglaciation models. The analysis selects the same lithospheric thickness and upper mantle viscosity in all cases, and the lower mantle viscosity varies between 10^{22} and $2 \times 10^{22} \text{ Pa s}$, indicating that our choice of optimum earth model is relatively robust and the uncertainty range given above is accurate. These results also confirm that the modelled ice-load changes in Antarctica are not of large enough spatial extent to excite extensive deformation in the lower mantle, and hence solutions are relatively insensitive to the value of viscosity in this region.

4.3 Adjusted model (Experiment 4)

Using the optimum earth model, uplift rates for the W12 deglaciation model are compared with elastic-corrected GPS-observed uplift rates (Figs 10a and b), and regions where the GIA model currently does not fit present-day geodetic observations are identified. The GIA model provides a good fit to the GPS data throughout East Antarctica (blue dots, Fig. 10b). Uplift rates at the Ross Sea sites (red dots, Fig. 10b) are only slightly over-predicted by the GIA model, except at ROB1, where the observed rate is $\sim 5 \text{ mm yr}^{-1}$ faster than the predicted rate; the velocity at this site appears to be erroneous as noted by Thomas *et al.* (2011). Throughout West Antarctica and the Antarctic Peninsula, the GIA model consistently predicts uplift rates that are greater than the observed rates (black and green dots, respectively, Fig. 10b). This is most notable along the Antarctic Peninsula where GPS rates approach zero after accounting for elastic rebound ($< 2 \text{ mm yr}^{-1}$), while the GIA model predicts rates of $\sim 5 \pm 2 \text{ mm yr}^{-1}$.

The W12 deglaciation model combined with the optimum earth model, as presented in Fig. 10(a), and is the main result of this study. The task of fine-tuning this model to fit the growing body of RSL and GPS data is largely a challenge for the future. However, in an attempt to improve the fit to observed uplift rates in the Antarctic Peninsula, a perturbed deglaciation model is constructed:

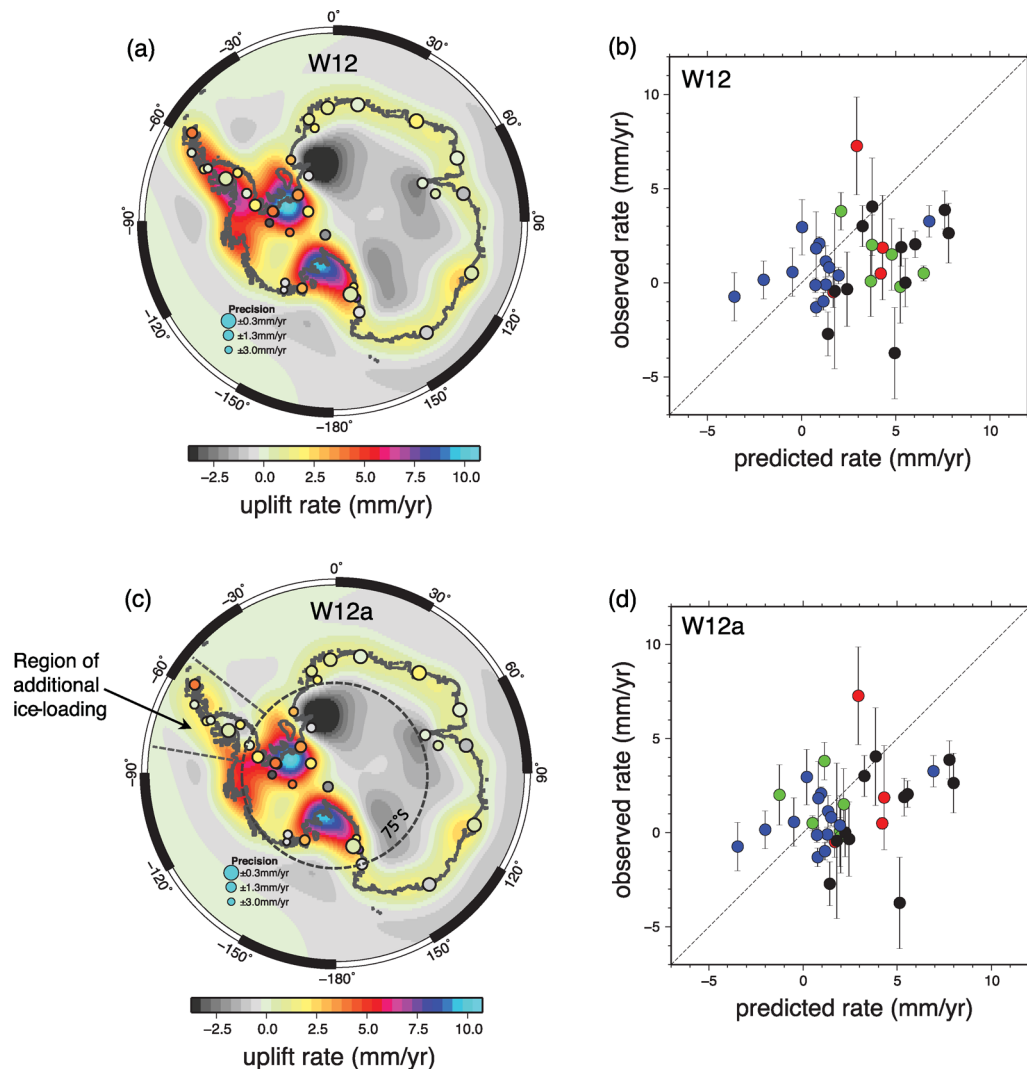


Figure 10. (a) Predicted uplift rates for the W12 deglacial model combined with the optimum earth model are overlain by elastic-corrected GPS rates (Thomas *et al.* 2011) plotted using the same colour scale. The magnitude of the circle at each GPS site is inversely proportional to the GPS uncertainty at that site (see Table S2). (b) Observed (elastic-corrected) versus predicted present-day uplift rates at the 35 GPS sites for the W12 deglacial model combined with the optimum earth model. Sites are colour-coded as in Figs 7(b) and 9(b). Vertical error bars are 1-sigma uncertainties for the GPS data. (c) As for (a), but for the W12a model. (d) As for (b) but for the W12a model.

The Late Holocene loading history in the Antarctic Peninsula is adjusted within the bounds of W12 model uncertainty and very sparse geological constraints. Ice-loading fluctuations are likely to have been considerable in the Antarctic Peninsula during this period of rapid climatic change (Vaughan *et al.* 2003), and will have a non-negligible effect upon present-day uplift rates (Ivins *et al.* 2000).

In line with observations of accumulation increases in the Antarctic Peninsula during the Late Holocene (Thomas *et al.* 2008), ice thickness increases between 10 and 500 m are applied between the 1000 a BP and 500 a BP time slices and/or the 500 a BP and 100 a BP time slices, with the possibility that the magnitude of additional loading is different in the East and West Antarctic Peninsula. The additional loading is applied anywhere there is grounded ice at the present-day in the region north of 75°S and between 280°E and 310°E. Within this the East Antarctic Peninsula is defined to be the region east of 295°E and south of 68°S. The ice-loading perturbation required to fit the weighted Antarctic Peninsula GPS data is found to be highly non-unique, and strongly dependent upon the adopted

earth model. For example, a smaller magnitude of additional ice would be required to fit the GPS data if a much weaker earth model were adopted for this region, as advocated by Ivins *et al.* (2011). Adopting the optimum earth model of Experiment 1, we find that increasing ice thicknesses throughout the Antarctic Peninsula (north of 75°S) by 150 m between the 1000 a BP and 500 a BP time slices, and by another 150 m between the 500 a BP and 100 a BP time slices, optimizes the fit to the weighted Antarctic Peninsula GPS data (Figs 10c, d, and Table S2). We call this ice model, which includes additional ice-loading in the Antarctic Peninsula during the Late Holocene, model W12a.

Using the W12a deglaciation model in conjunction with the optimum earth model, the WRMS error for GPS sites within West Antarctica improves from 4.2 to 3.1 mm yr⁻¹, and the WRMS error for the full set of Antarctic GPS sites improves from 2.9 to 2.3 mm yr⁻¹. The mean bias, for the full set of sites, is reduced from 1.8 to 1.2 mm yr⁻¹, indicating that predicted uplift rates based on the W12a model, when combined with the optimum earth model, are still biased high compared with the observed uplift rates.

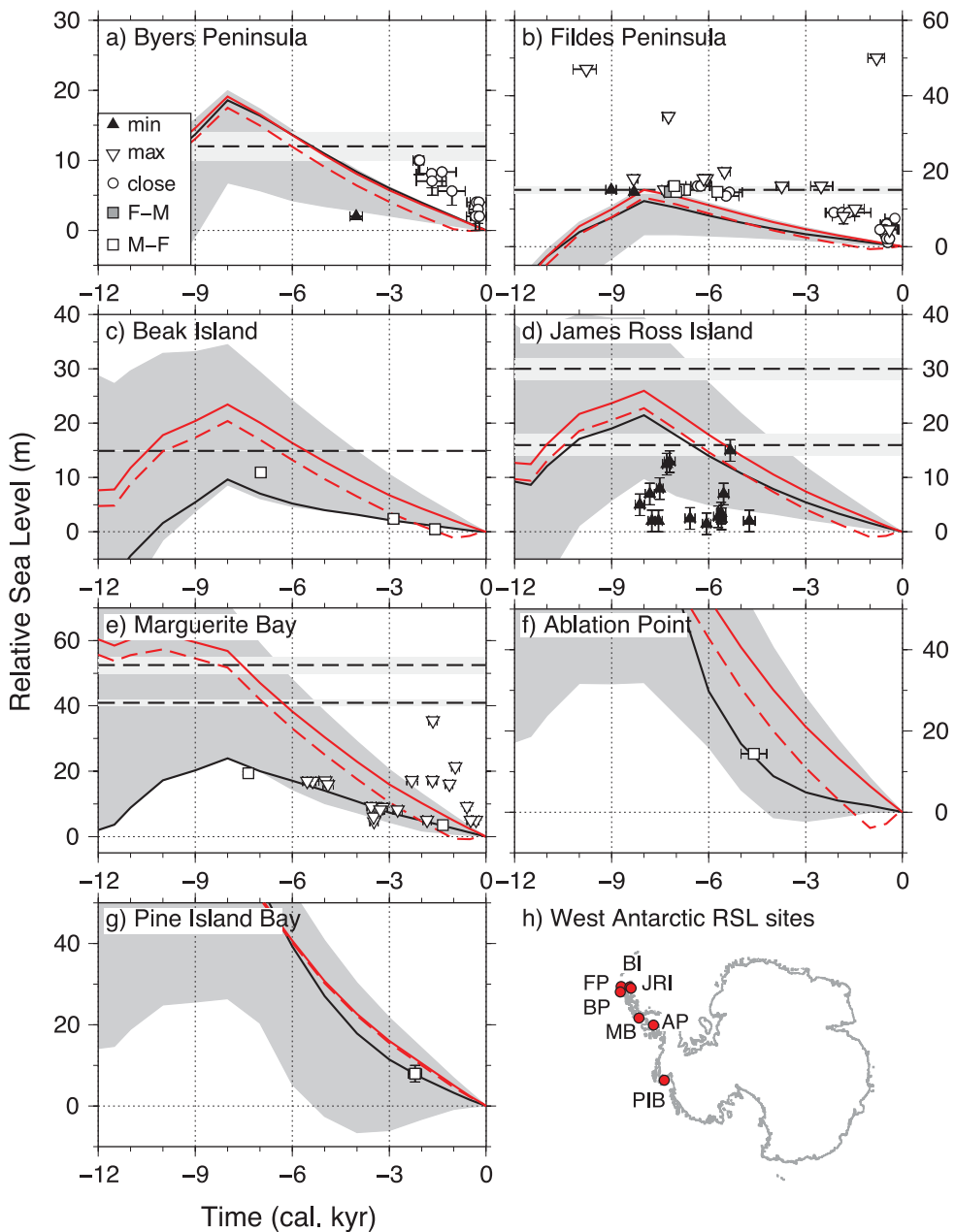


Figure 11. RSL data and predictions at Antarctic Peninsula sites. Fig. 11 is identical to Fig. 3 apart from the addition of predicted RSL curves for the W12a deglaciation model at each site (red dashed lines). These predictions are generated using the same (optimum) earth model as the solid red lines (W12 deglaciation model).

The perturbation to the W12 ice-loading history required to produce the W12a deglaciation model does not affect RSL predictions for East Antarctica or the Ross Sea, but it does have an impact upon RSL predictions in the Antarctic Peninsula (Fig. 11): the magnitude of the predicted Holocene highstand is decreased by up to 3 m, and RSL predictions approach present-day levels 1–2 ka BP, with some sites predicted to have experienced RSL below present during the last 1000 yr. This pattern of RSL change arises as background rates of rebound, due to Holocene unloading, are balanced by subsidence due to the increase in loading during the last millennium. The resolution of the RSL data is currently too low to be able to test the validity of these perturbations to the RSL predictions, but the data do not exclude the W12a deglaciation model and the GPS

data require the lower rates of uplift provided by this modification; other variants may provide similar or better fits.

4.4 Uncertainty in modelled uplift rates

For the calculations of Section 4.3, the optimum earth model of Experiment 1 is used, but we note that the W12a model displays a similar sensitivity to earth model uncertainty as the W12 model. We now seek the earth models that provide lower and upper bounds on the maximum rate of GIA-related geoid height change within Antarctica when combined with the W12 and W12a deglaciation histories. Geoid heights are used to define these bounds since the primary goal of this study is to provide a bounded GIA correction to

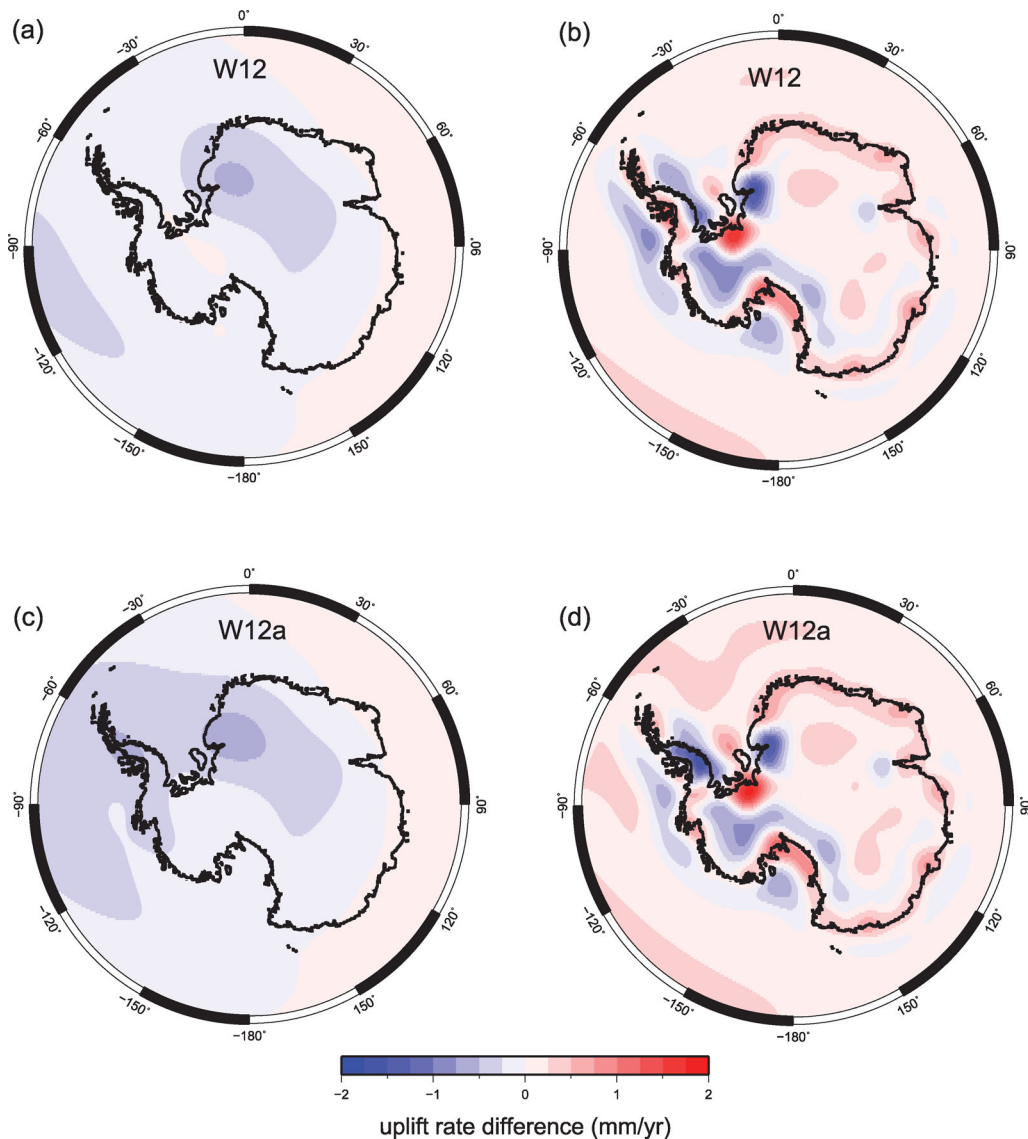


Figure 12. W12 model range: (a) uplift rates for the lower bound earth model (see main text) minus uplift rates for the optimum earth model (Fig. 10a). (b) Uplift rates for the upper bound earth model (see main text) minus uplift rates for the optimum earth model (Fig. 10a). (c) As for (a), but for the W12a model. (d) As for (b), but for the W12a model.

the GRACE data. However, for consistency with previous figures, we plot uplift rates relating to these lower and upper bound solutions in Fig. 12. Earth models are chosen from within the 95 per cent confidence limits of Experiment 1.

In Fig. 12 we plot the difference between predicted uplift rates for the W12/W12a model combined with the optimum earth model (Figs 10a and c) and predicted uplift rates for earth models that define lower and upper bounds for the W12/W12a models. These difference plots may be regarded as the uncertainty, expressed in terms of uplift rates, associated with the W12 and W12a models. The shorter wavelength signal in Figs 12(b)/(d), compared to Figs 12(a)/(c), is associated with the fact that earth models with different lithospheric thicknesses are differenced to produce the former plots. The parameter space has also been expanded to include different deglaciation histories, as described in Experiment 3 (Section 4.2.2). This slightly alters the pattern of the spatially variable uncertainty, but, to first order, it does not alter the mag-

nitude due to trade-offs between the ice/earth model combinations that give a good fit to the RSL data. In general, uncertainty on uplift is $\sim 2 \text{ mm yr}^{-1}$ in West Antarctica and $\sim 1 \text{ mm yr}^{-1}$ throughout the majority of East Antarctica.

The lower bound for both the W12 and W12a models (Figs 12a and c) is provided by an earth model with a lithospheric thickness of 120 km, an upper mantle viscosity of $1 \times 10^{21} \text{ Pa s}$, and a lower mantle viscosity of $5 \times 10^{21} \text{ Pa s}$. The upper bound for both the W12 and W12a models (Figs 12b and d) is provided by an earth model with a lithospheric thickness of 96 km, an upper mantle viscosity of $0.8 \times 10^{21} \text{ Pa s}$, and a lower mantle viscosity of $20 \times 10^{21} \text{ Pa s}$. This limiting method is used to define the uncertainty in our solutions, instead of simply adopting the total range of uplift rates at each point, because these upper and lower bound solutions are physically self-consistent solutions to the sea-level equation, and hence can be used to directly constrain the error on the GIA correction that will be applied to the GRACE data.

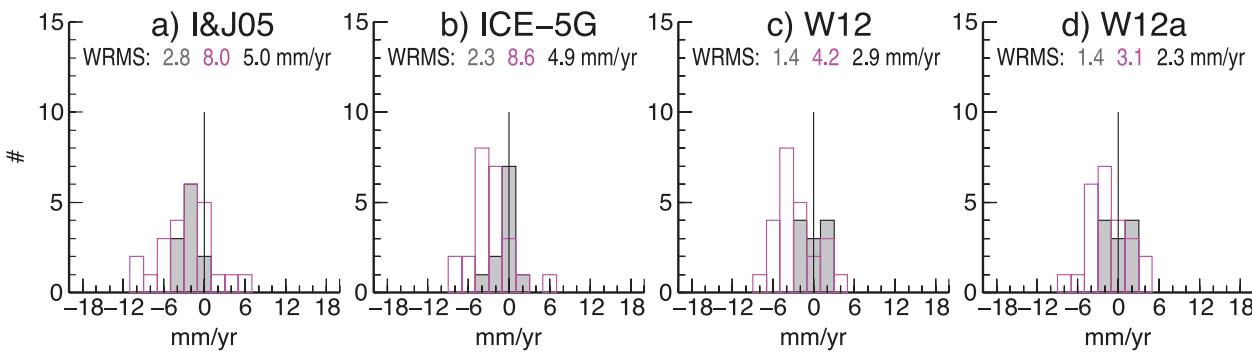


Figure 13. Histograms of GPS-observed (elastic corrected) minus model uplift rates for East (grey) and West (magenta) Antarctica for the IJ05, ICE-5G, W12 and W12a models. W12 and W12a predictions are calculated using the optimum earth model (see main text). Weighted Root-Mean-Square (WRMS, weights based on uncertainties in Table S2) values are also given, including the WRMS for all sites (black).

5 DISCUSSION

Our new GIA model is a clear improvement upon previous attempts to model GIA processes in Antarctica, demonstrating an improved fit to available RSL and GPS data sets (Figs 3, 10 and 13; cf. Bassett *et al.* 2007; Thomas *et al.* 2011). Our best-fit deglaciation model, W12, uses a stepped model of ice retreat, in agreement with geological observations. To give the best fit to RSL observations, the W12 model is combined with our optimum earth model, which has a lithospheric thickness of 120 km, an upper mantle viscosity of 1×10^{21} Pa s, and a lower mantle viscosity of 5×10^{21} Pa s.

The W12 deglaciation history accurately reproduces the majority of the RSL observations when coupled with the best-fitting earth model specific to each site. At almost all sites, the model-data agreement decreases when a single earth model is used to calculate RSL predictions at all sites, or a subset of sites (red and blue lines on Fig. 3). At several sites (Beak Island, Marguerite Bay, Ablation Point, Vestfold Hills, and Larsemann Hills) the shape of the predicted RSL curve is highly sensitive to the choice of upper mantle viscosity, making it impossible to simultaneously fit the data at these sites using a single earth model. This may reflect lateral variations in rheological properties, but in the central Antarctic Peninsula, where best-fitting site-specific upper mantle viscosities vary $0.1\text{--}5 \times 10^{21}$ Pa s within ~ 300 km, it likely reflects errors in the ice-loading history. For this reason, we omit the Marguerite Bay RSL data to prevent bias in our search for those earth models that best reproduce the Antarctic RSL data set. The fit to RSL data may be further improved by adopting a different eustatic model.

The W12 deglaciation history, when combined with the optimum earth model, accurately reproduces present-day uplift rates throughout the majority of Antarctica (Fig. 10a). There is a clear improvement in the fit between observed and predicted uplift rates at the Antarctic Peninsula sites when we attempt to account for Late Holocene loading (model W12a, green dots, Fig. 10d), and we caution that the ice-loading history of the original W12 deglaciation model probably contains large errors in this region. Inaccuracies in the deglaciation model are likely related to the spatial resolution of the numerical ice-sheet model and the inability of the physics used within this model to represent steep lateral gradients in ice velocity. In addition, the very different mantle rheology of the northern Antarctic Peninsula (Ivins *et al.* 2011) adds to the complexity of modelling GIA in this region.

The WRMS error for our W12 and W12a modelled uplift rates, calculated using the optimum earth model, is $\sim 2\text{--}2.5$ mm yr $^{-1}$ smaller than for the IJ05 and ICE-5G GIA models (Fig. 13, weights are based on GPS uncertainties). However, our predicted uplift rates

are still biased high (Figs 13c and d) and Fig. 10(c) shows remaining areas of misfit to be around the southern Weddell Sea coast. The mean misfit can be reduced by choosing a very low ($\sim 10^{19}$ Pa s), or very high (5×10^{21} Pa s), upper mantle viscosity for the whole of Antarctica, but such earth models would be unable to reproduce the RSL observations, and are incompatible with independent estimates of upper mantle viscosities for continental regions (Lambeck & Chappell 2001; Mitrovica & Forte 2004). The remaining misfit may reflect our inability to represent lateral variations in Earth structure (Morelli & Danesi 2004), which would, incidentally, have a profound effect upon horizontal rates of deformation (Kaufmann *et al.* 2005). The misfit may also have some contribution from GPS velocity errors, including those related to the modelling of elastic effects, but it is most likely that the high uplift rates reflect the presence of too much ice in the W12 ice-sheet reconstruction during the LGM in this region (Whitehouse *et al.* 2012).

We have demonstrated that neither the early loading history (prior to ~ 50 ka BP) nor the rate of deglaciation prior to 5 ka BP has a measurable effect upon present-day uplift rates. However, the timing, duration and magnitude of the LGM, and, crucially, the details of ice loading during the last 5 ka (Ivins *et al.* 2000), can perturb present-day uplift rates by 1–2 mm yr $^{-1}$ (e.g. Fig. 8d). A signal of this magnitude is measurable given the current vertical precision of GPS measurements, and therefore these characteristics of the AIS must be more tightly constrained in future ice-sheet reconstructions. In particular, the degree to which the LGM was a long-lived, Antarctic-wide, contemporaneous event should be investigated. For example, uplift rate predictions would be considerably reduced if the maximum extent of the dynamic, marine-grounded West AIS was a transient state, only maintained for a few thousand years.

The optimum earth model, which was chosen to give the best fit to the RSL data, lies within the range of viscosity models proposed by earlier GIA studies (Nakada & Lambeck 1988; Ivins & James 2005). However, the earth models preferred by the subsets of East and West Antarctic sites contain some surprising features: The East Antarctic data prefer an earth model with a lithospheric thickness of 71 km, in disagreement with the general consensus that this region is underlain by very thick lithosphere (Ritzwoller *et al.* 2001; Morelli & Danesi 2004). In addition, these data prefer a lower mantle viscosity of 2×10^{21} Pa s. This value is only double the upper mantle viscosity value preferred by the East Antarctic RSL data, at odds with the view that lower mantle viscosities are at least an order of magnitude greater than upper mantle viscosities (Mitrovica 1996; Lambeck *et al.* 1998; Mitrovica & Forte 2004). However, there is only a weak dependence upon these parameters for this subset of data, so the preference for a thin lithosphere and a relatively weak lower mantle is not completely

robust. More surprising is the result that the West Antarctic RSL data prefer a similar upper mantle viscosity to East Antarctica, in disagreement with the general consensus that the upper mantle is hot and weak in this former rift zone (Ritzwoller *et al.* 2001; Morelli & Danesi 2004). If the Ross Sea RSL sites are redefined to be ‘East Antarctic sites’ this does not alter the result, and the χ^2 misfit for the West Antarctic sites does not appreciably improve. It will be interesting to see whether the upper mantle viscosities preferred by the RSL data are supported by forthcoming seismic data (www.polenet.org). As discussed earlier, these regional earth model solutions may be biased by errors in the ice-loading history, but they will also be influenced by sites which have a very small number of data, as these will have a strong preference for a small subset of earth models. Low quality RSL data that have poor age constraints, or are open to incorrect interpretation, may also bias the choice of earth model. The improvement and expansion of the RSL data set for Antarctica would have a profound effect upon our ability to constrain local Earth rheology and regional ice-loading histories since the LGM.

The error bars attached to our GIA model are related to uncertainty in both the deglacial reconstruction and the earth model (Figs 7–9 and 12), and the greatest errors are found in regions of greatest uplift. There is a strong trade-off between ice loading and upper mantle viscosity in such regions, and it is imperative that maximum uplift rates are constrained as tightly as possible. Unfortunately there are few outcrops in these regions of rapid uplift upon which to establish GPS sites, and there are still extensive areas throughout Antarctica where our GIA model contains large uncertainties due to a lack of GPS or RSL data to test different scenarios. The collection of such data is limited by the low density of rock outcrops in many regions, but areas such as Dronning Maud Land and Coats Land (where, interestingly, up to 6 mm yr^{-1} present-day subsidence is predicted by our best-fitting model) have the potential to provide vital information on the deglacial history of the AIS, and hence reduce GIA model uncertainties. The seismic profiling carried out during the POLENET project (www.polenet.org) should also help to address questions relating to uncertainty in Earth structure.

In creating our adjusted deglaciation model, W12a, we attempt to generate a GIA model that best fits available geodetic observations of GIA-related uplift, and hence provide the most accurate GIA correction possible to the GRACE community. We note that this approach is dependent upon our ability to accurately account for the elastic response to present-day loading within the GPS data (Thomas *et al.* 2011), and suggest that an iterative or inverse approach to this problem should be considered in future work. The method that we have used to reduce predicted uplift rates in the Antarctic Peninsula may not accurately capture all of the physical processes taking place. Indeed, the IJ05 model (Ivins & James 2005) invokes a much smaller LGM ice sheet in the northern Antarctic Peninsula, and achieves a good fit to the GPS data in this region (Thomas *et al.* 2011), whereas Ivins *et al.* (2011) invoke low mantle viscosities to fit an alternative set of GPS data.

Finally, we compare our new Antarctic GIA model results with existing models, which have thus far been used to correct the GRACE data. Our predicted uplift rates display a similar large-scale pattern to those in the IJ05 model (Ivins & James 2005; Simon *et al.* 2010; Fig. 14), with subsidence in the interior of East Antarctica and uplift throughout West Antarctica. Maximum uplift rates for these two models are of the same order of magnitude, but we predict strong uplift in the Weddell Sea, while the IJ05 model predicts strong uplift in the southern Antarctic Peninsula, which seems to

be at odds with the GPS data. Our prediction of low ($\sim 1 \text{ mm yr}^{-1}$) uplift rates around the coast of East Antarctica is also in better agreement with the GPS data than the IJ05 model. The ICE-5G model (Peltier 2004) predicts uplift in the interior of East Antarctica, and whilst this cannot be refuted by the GPS data, it is in disagreement with observations of lower LGM elevations in this region of the ice sheet, as derived from ice core data (Jouzel *et al.* 1989; Parrenin *et al.* 2007). Maximum uplift rates predicted by the ICE-5G model are greater than those predicted by our model, especially along the Siple Coast. This issue, again, cannot be resolved due to the lack of uplift rate observations in this region, but constraints on former ice thicknesses in this region (Whitehouse *et al.* 2012, and references therein) indicate that even the W12 model thickness changes are an upper bound, and therefore the ICE-5G rates are likely an over-estimate.

The differences between these three models highlight the difficulty of creating an accurate GIA model for Antarctica, and we therefore place spatially-variable upper and lower bounds on our final solution (Fig. 12). Errors have been assessed due to uncertainties in both the ice-loading history and the earth model parameters, and should be used to place bounds on the GIA contribution to the GRACE data.

6 CONCLUSIONS

(1) We present a new GIA model for Antarctica, which is driven by a new deglaciation history that has been developed using a numerical ice-sheet model and tuned to fit observations of ice extent since the LGM.

(2) There is no single earth model that simultaneously fits the RSL data well at all sites, however, a good fit with field observations around Antarctica can be achieved for a small range of earth models. The predictions are only weakly dependent upon changes in lithospheric thickness and lower mantle viscosity and so useful constraints on these parameters could not be determined. In contrast, the predictions are sensitive to changes in upper mantle viscosity and the RSL data constrain this parameter to lie in the range (95 per cent confidence) $0.8\text{--}2.0 \times 10^{21} \text{ Pa s}$.

(3) We attribute misfits to the RSL data to errors in the deglaciation history, or the unmodelled effects of lateral Earth structure. Improvements in the quality of the RSL data may also improve the fit.

(4) Comparing GIA model predictions to elastic-corrected GPS uplift rates we find that our W12 model predictions, generated using the optimum earth model, are biased high (mean bias = 1.8 mm yr^{-1}), and we calculate a WRMS of 2.9 mm yr^{-1} . GPS rates in East Antarctica are accurately reproduced by the W12 model, but uplift rates are systematically over-predicted by this model in some areas of West Antarctica and throughout the Antarctic Peninsula. The GPS data are best-fit by an earth model very similar to that preferred by the RSL data.

(5) We find a weak dependence of present-day uplift rates on the details of the deglaciation history prior to 5 ka BP. We therefore address the misfit to GPS uplift rates in the Antarctic Peninsula by adjusting only the Late Holocene loading history in this region, within the bounds of uncertainty of the deglaciation model. Using this adjusted model (model W12a), in combination with the optimum earth model, the WRMS error for West Antarctica improves from 4.2 to 3.1 mm yr^{-1} and the WRMS considering all Antarctic GPS sites improves from 2.9 to 2.3 mm yr^{-1} . The weighted mean bias across Antarctica is reduced from 1.8 to 1.2 mm yr^{-1} .

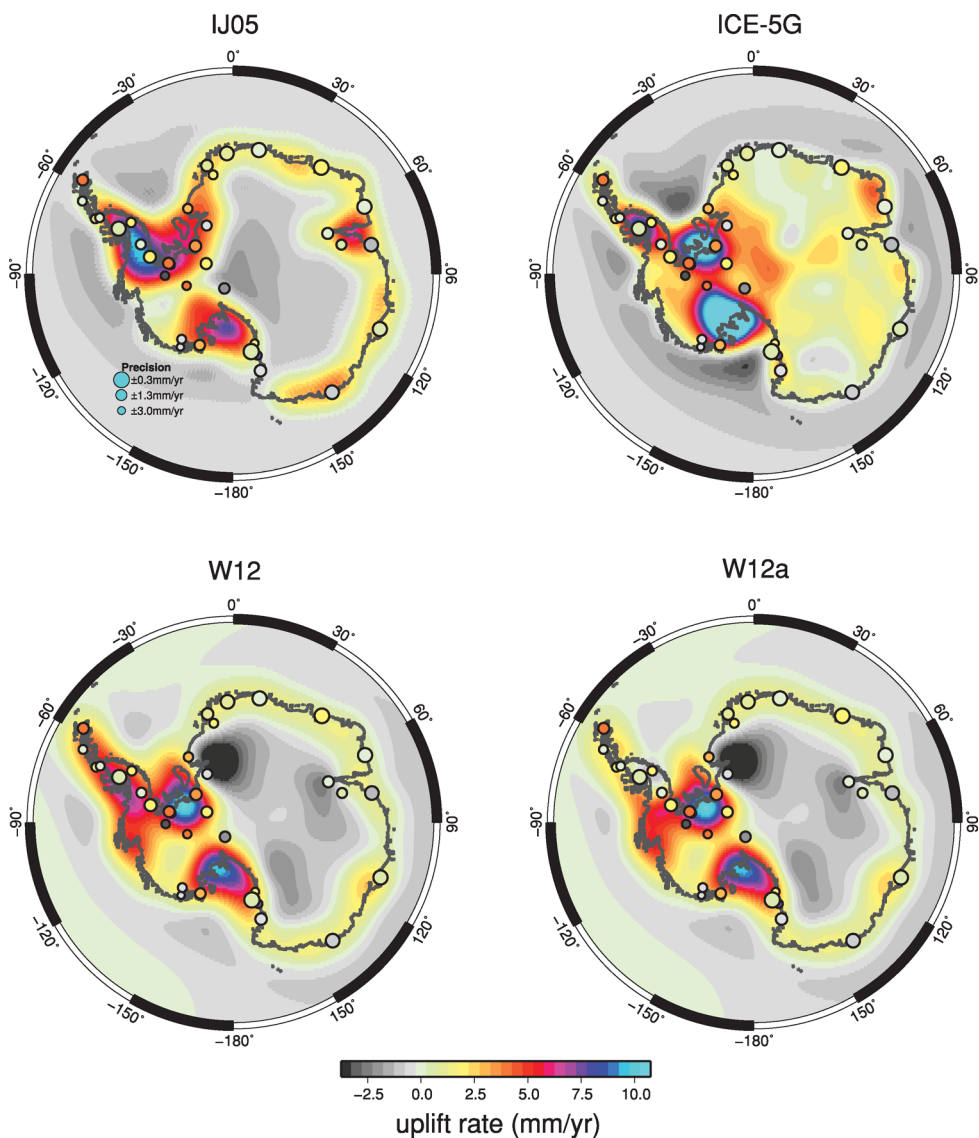


Figure 14. Present-day uplift rate predictions for the IJ05, ICE-5G, W12 and W12a GIA models. W12 and W12a predictions are calculated using the optimum earth model (see main text). Elastic-corrected GPS rates (Thomas *et al.* 2011) are plotted using the same colour scale, and the magnitude of the circle at each GPS site is inversely proportional to the GPS uncertainty at that site.

(6) Our WRMS error of 2.3 mm yr^{-1} (model W12a, optimum earth model) is an improvement upon the values of 4.9 mm yr^{-1} for ICE-5G and 5.0 mm yr^{-1} for IJ05. Our predicted uplift rate distribution is similar to IJ05, but we find a smaller magnitude of uplift around coastal East Antarctica and in the southern Antarctic Peninsula. Similar to ICE-5G we predict the greatest uplift rates in the Ross and Weddell Seas, although our maxima are smaller than predicted by ICE-5G.

(7) We quantify errors on our predicted GIA uplift rates due to uncertainties in both the ice-loading history and the adopted earth model. Improving the Antarctic RSL and GPS datasets would decrease these uncertainties. Spatially variable error bars are placed on our final GIA uplift rate predictions, thus providing an invaluable tool for the future quantification of ice-mass change in Antarctica by geodetic, altimetric, and gravitational methods.

(8) This work provides a new GIA correction for the GRACE data in Antarctica, thus permitting more accurate constraints to be placed on current ice-mass change.

ACKNOWLEDGEMENTS

This work was carried out under NERC grants NE/E004806/1 and NE/E007023/1. It was also supported by COST Action ES0701, and a RCUK Academic Fellowship to MAK. GAM acknowledges support from the Natural Sciences and Engineering Research Council of Canada and the Canada Research Chairs program. We thank Erik Ivins and W. Richard Peltier for providing their models, the editor for his assistance, and Erik Ivins and an anonymous reviewer for their constructive comments.

REFERENCES

- Adamson, D.A., Mabin, M.C.G. & Luly, J.G., 1997. Holocene isostasy and late Cenozoic development of landforms including Beaver and Radok Lake basins in the Amery Oasis, Prince Charles Mountains, Antarctica, *Antarct. Sci.*, **9**, 299–306.
- Andrews, J.T., 1970. *A Geomorphological Study of Postglacial Uplift with Particular Reference to Arctic Canada*, Spec. Pub. No. 2, Institute of British Geographers, London.

- Argus, D.F., Blewitt, G., Peltier, W.R. & Kreemer, C., 2011. Rise of the Ellsworth mountains and parts of the East Antarctic coast observed with GPS, *Geophys. Res. Lett.*, **38**, L161303, doi:10.1029/2011GL048025.
- Baroni, C. & Hall, B.L., 2004. A new Holocene relative sea-level curve for Terra Nova Bay, Victoria Land, Antarctica, *J. Quat. Sci.*, **19**, 377–396.
- Bassett, S.E., Milne, G.A., Bentley, M.J. & Huybrechts, P., 2007. Modelling Antarctic sea-level data to explore the possibility of a dominant Antarctic contribution to meltwater pulse IA, *Quat. Sci. Rev.*, **26**, 2113–2127.
- Bassett, S.E., Milne, G.A., Mitrovica, J.X. & Clark, P.U., 2005. Ice sheet and solid earth influences on far-field sea-level histories, *Science*, **309**, 925–928.
- Bentley, M.J., Hodgson, D.A., Smith, J.A. & Cox, N.J., 2005. Relative sea level curves for the South Shetland Islands and Marguerite Bay, Antarctic Peninsula, *Quat. Sci. Rev.*, **24**, 1203–1216.
- Berg, S., Wagner, B., Cremer, H., Leng, M.J. & Melles, M., 2010. Late Quaternary environmental and climate history of Rauer Group, East Antarctica, *Palaeogeogr. Palaeoclimat. Palaeoecol.*, **297**, 201–213.
- Bevis, M. et al., 2009. Geodetic measurements of vertical crustal velocity in West Antarctica and the implications for ice mass balance, *Geochem. Geophys. Geosyst.*, **10**, Q10005, doi:10.1029/2009GC002642.
- Björck, S., Hjort, C., Ingólfsson, Ó. & Skog, G., 1991. Radiocarbon dates from the Antarctic Peninsula region – problems and potential, *Quat. Proc.*, **1**, 55–65.
- Björck, S., Hjort, C., Ingólfsson, Ó., Zale, R. & Ising, J., 1996. Holocene deglaciation chronology from lake sediments, in *Geomorphological Map of Byers Peninsula, Livingston Island*, pp. 49–51, eds López-Martínez, J. et al., Sheet 45-A, 41:25 000 with supplementary text, British Antarctic Survey, Cambridge.
- Bradley, S.L., Milne, G.A., Zong, Y. & Horton, B., 2008. Modelling sea-level data from China and Malay-Thai Peninsula to infer Holocene eustatic sea-level change. American Geophysical Union, Fall Meeting 2008, abstract # GC33A-0763.
- Chen, J.L., Wilson, C.R., Blankenship, D. & Tapley, B.D., 2009. Accelerated Antarctic ice loss from satellite gravity measurements, *Nat. Geosci.*, **2**, 859–862.
- Chen, J.L., Wilson, C.R., Blankenship, D.D. & Tapley, B.D., 2006. Antarctic mass rates from GRACE, *Geophys. Res. Lett.*, **33**, L11502, doi:10.1029/2006GL026369.
- Chen, J.L., Wilson, C.R., Tapley, B.D., Blankenship, D. & Young, D., 2008. Antarctic regional ice loss rates from GRACE, *Earth planet. Sci. Lett.*, **266**, 140–148.
- Dziewonski, A.M. & Anderson, D.L., 1981. Preliminary Reference Earth Model, *Phys. Earth planet. Inter.*, **25**, 297–356.
- ETOPO2v2, 2006. ETOPO2v2 Global Gridded 2-minute Database, National Geophysical Data Center, National Oceanic and Atmospheric Administration, U.S. Dept. of Commerce, Available at: <http://www.ngdc.noaa.gov/mgg/global/etopo2.html> (last accessed 2009).
- Farrell, W.E. & Clark, J.A., 1976. On postglacial sea level, *Geophys. J. R. astr. Soc.*, **46**, 647–667.
- Goodwin, I.D., 1993. Holocene deglaciation, sea-level change, and the emergence of the windmill islands, Budd Coast, Antarctica, *Quat. Res.*, **40**, 70–80.
- Goodwin, I.D. & Zweck, C., 2000. Glacio-isostasy and glacial ice load at Law Dome, Wilkes Land, East Antarctica, *Quat. Res.*, **53**, 285–293.
- Hjort, C., Ingolfsson, O., Moller, P. & Lirio, J.M., 1997. Holocene glacial history and sea-level changes on James Ross Island, Antarctic Peninsula, *J. Quat. Sci.*, **12**, 259–273.
- Huybrechts, P., 2002. Sea-level changes at the LGM from ice-dynamic reconstructions of the Greenland and Antarctic ice sheets during the glacial cycles, *Quat. Sci. Rev.*, **21**, 203–231.
- Ivins, E.R. & James, T.S., 2005. Antarctic glacial isostatic adjustment: a new assessment, *Antarct. Sci.*, **17**, 541–553.
- Ivins, E.R., Raymond, C.A. & James, T.S., 2000. The influence of 5000 year-old and younger glacial mass variability on present-day crustal rebound in the Antarctic Peninsula, *Earth Planets Space*, **52**, 1023–1029.
- Ivins, E.R., Watkins, M.M., Yuan, D.-N., Dietrich, R., Casassa, G. & Rülke, A., 2011. On-land ice loss and glacial isostatic adjustment at the Drake Passage: 2003–2009, *J. geophys. Res.*, **116**, B02403.
- Johnson, J.S., Bentley, M.J. & Gohl, K., 2008. First exposure ages from the Amundsen Sea embayment, West Antarctica: the late quaternary context for recent thinning of Pine Island, Smith, and Pope Glaciers, *Geology*, **36**, 223–226.
- Jouzel, J. et al., 1989. A comparison of deep Antarctic ice cores and their implications for climate between 65,000 and 15,000 years ago, *Quat. Res.*, **31**, 135–150.
- Kaufmann, G., Wu, P. & Ivins, E.R., 2005. Lateral viscosity variations beneath Antarctica and their implications on regional rebound motions and seismotectonics, *J. Geodyn.*, **39**, 165–181.
- Kendall, R.A., Mitrovica, J.X. & Milne, G.A., 2005. On post-glacial sea level — II. Numerical formulation and comparative results on spherically symmetric models, *Geophys. J. Int.*, **161**, 679–706.
- Klemann, V. & Martinec, Z., 2011. Contribution of glacial-isostatic adjustment to the geocenter motion, *Tectonophysics*, **511**, 99–108.
- Kopp, R.E., Simons, F.J., Mitrovica, J.X., Maloof, A.C. & Oppenheimer, M., 2009. Probabilistic assessment of sea level during the last interglacial stage, *Nature*, **462**, U863–U851.
- Lambeck, K. & Chappell, J., 2001. Sea level change through the last glacial cycle, *Science*, **292**, 679–686.
- Lambeck, K., Smither, C. & Johnston, P., 1998. Sea-level change, glacial rebound and mantle viscosity for northern Europe, *Geophys. J. Int.*, **134**, 102–144.
- Le Brocq, A.M., Payne, A.J. & Vieli, A., 2010. An improved Antarctic dataset for high resolution numerical ice sheet models (ALBMAP v1), *Earth System Sci. Data*, **2**, 247–260.
- Liu, J.P. & Milliman, J.D., 2004. Reconsidering melt-water pulses 1A and 1B: global impacts of rapid sea-level rise, *J. Ocean Univ. China*, **3**, 183–190.
- Milne, G.A. & Mitrovica, J.X., 1998. Postglacial sea-level change on a rotating Earth, *Geophys. J. Int.*, **133**, 1–19.
- Milne, G.A., Mitrovica, J.X. & Davis, J.L., 1999. Near-field hydro-isostasy: the implementation of a revised sea-level equation, *Geophys. J. Int.*, **139**, 464–482.
- Mitrovica, J.X., 1996. Haskell [1935] revisited, *J. geophys. Res.*, **101**, 555–569.
- Mitrovica, J.X. & Davis, J.L., 1995. The influence of a finite glaciation phase on predictions of post-glacial isostatic adjustment, *Earth planet. Sci. Lett.*, **136**, 343–361.
- Mitrovica, J.X. & Forte, A.M., 2004. A new inference of mantle viscosity based upon joint inversion of convection and glacial isostatic adjustment data, *Earth planet. Sci. Lett.*, **225**, 177–189.
- Mitrovica, J.X. & Milne, G.A., 2003. On post-glacial sea level: I. General theory, *Geophys. J. Int.*, **154**, 253–267.
- Mitrovica, J.X., Wahr, J., Matsuyama, I. & Paulson, A., 2005. The rotational stability of an ice-age earth, *Geophys. J. Int.*, **161**, 491–506.
- Morelli, A. & Danesi, S., 2004. Seismological imaging of the Antarctic continental lithosphere: a review, *Global planet. Change*, **42**, 155–165.
- Nakada, M., Kimura, R., Okuno, J., Moriwaki, K., Miura, H. & Maemoku, H., 2000. Late Pleistocene and Holocene melting history of the Antarctic ice sheet derived from sea-level variations, *Mar. Geol.*, **167**, 85–103.
- Nakada, M. & Lambeck, K., 1988. The melting history of the late pleistocene antarctic ice-sheet, *Nature*, **333**, 36–40.
- Parrenin, F. et al., 2007. 1-D-ice flow modelling at EPICA Dome C and Dome Fuji, East Antarctica, *Clim. Past*, **3**, 243–259.
- Peltier, W.R., 2004. Global glacial isostasy and the surface of the ice-age earth: the ICE-5G (VM2) model and GRACE, *Annu. Rev. Earth planet. Sci.*, **32**, 111–149.
- Pollard, D. & DeConto, R.M., 2009. Modelling West Antarctic ice sheet growth and collapse through the past five million years, *Nature*, **458**, 329–389.
- Ramillien, G., Lombard, A., Cazenave, A., Ivins, E.R., Llubes, M., Remy, F. & Biancale, R., 2006. Interannual variations of the mass balance of the Antarctica and Greenland ice sheets from GRACE, *Global planet. Change*, **53**, 198–208.
- Rietbroek, R., Brunnabend, S.-E., Kusche, J. & Schröter, J., 2011. Resolving sea level contributions by identifying fingerprints in time-variable gravity and altimetry, *J. Geodyn.*, in press, doi:10.1016/j.jog.2011.06.007.

- Rignot, E., Casassa, G., Gogineni, P., Krabill, W., Rivera, A. & Thomas, R., 2004. Accelerated ice discharge from the Antarctic Peninsula following the collapse of Larsen B ice shelf, *Geophys. Res. Lett.*, **31**, L18401, doi:10.1029/2004GL020697.
- Ritz, C., Rommelaere, V. & Dumas, C., 2001. Modeling the evolution of Antarctic ice sheet over the last 420,000 years: implications for altitude changes in the Vostok region, *J. geophys. Res.*, **106**, 31 943–31 964.
- Ritzwoller, M.H., Shapiro, N.M., Levshin, A.L. & Leahy, G.M., 2001. Crustal and upper mantle structure beneath Antarctica and surrounding oceans, *J. geophys. Res.*, **106**, 30 645–30 670.
- Riva, R.E.M. et al., 2009. Glacial Isostatic Adjustment over Antarctica from combined ICESat and GRACE satellite data, *Earth planet. Sci. Lett.*, **288**, 516–523.
- Roberts, S.J., Hodgson, D.A., Bentley, M.J., Sanderson, D.C.W., Milne, G., Smith, J.A., Verleyen, E. & Balbo, A., 2009. Holocene relative sea-level change and deglaciation on Alexander Island, Antarctic Peninsula, from elevated lake deltas, *Geomorphology*, **112**, 122–134.
- Roberts, S.J. et al., 2011. Geological constraints on glacio-isostatic adjustment models of relative sea-level change during deglaciation of Prince Gustav Channel, Antarctic Peninsula, *Quat. Sci. Rev.*, **30**, 3603–3617.
- Rutt, I.C., Haggorn, M., Hulton, N.R.J. & Payne, A.J., 2009. The Glimmer community ice sheet model, *J. geophys. Res.*, **114**, F02004, doi:10.1029/2008JF001015.
- Simms, A.R., Milliken, K.T., Anderson, J.B. & Wellner, J.S., 2011. The marine record of deglaciation of the South Shetland Islands, Antarctica since the Last Glacial Maximum, *Quat. Sci. Rev.*, **30**, 1583–1601.
- Simon, K.M., James, T.S. & Ivins, E.R., 2010. Ocean loading effects on the prediction of Antarctic glacial isostatic uplift and gravity rates, *J. Geodyn.*, **84**, 305–317.
- Thomas, E.R., Marshall, G.J. & McConnell, J.R., 2008. A doubling in snow accumulation in the western Antarctic Peninsula since 1850, *Geophys. Res. Lett.*, **35**, L01706, doi:10.1029/2007GL032529.
- Thomas, I.D. et al., 2011. Widespread low rates of Antarctic glacial isostatic adjustment revealed by GPS observations, *Geophys. Res. Lett.*, **38**, L22302, doi:10.1029/2011GL049277.
- Vaughan, D.G. et al., 2003. Recent rapid regional climate warming on the Antarctic Peninsula, *Clim. Change*, **60**, 243–274.
- Velicogna, I., 2009. Increasing rates of ice mass loss from the Greenland and Antarctic ice sheets revealed by GRACE, *Geophys. Res. Lett.*, **36**, L19503, doi:10.1029/2009GL040222.
- Velicogna, I. & Wahr, J., 2006. Measurements of time-variable gravity show mass loss in Antarctica, *Science*, **311**, 1754–1756.
- Wagner, B., Hultsch, N., Melles, M. & Gore, D.B., 2007. Indications of holocene sea-level rise in Beaver Lake, East Antarctica, *Antarct. Sci.*, **19**, 125–128.
- Watcham, E.P. et al., 2011. A new Holocene relative sea level curve for the South Shetland Islands, Antarctica, *Quat. Sci. Rev.*, **30**, 3152–3170.
- Whitehouse, P.L., Bentley, M.J. & Le Brocq, A.M., 2012. A deglacial model for Antarctica: geological constraints and glaciological modelling as a basis for a new model of Antarctic glacial isostatic adjustment, *Quat. Sci. Rev.*, **32**, 1–24.
- Wu, X.P. et al., 2010. Simultaneous estimation of global present-day water transport and glacial isostatic adjustment, *Nat. Geosci.*, **3**, 642–646.

SUPPORTING INFORMATION

Additional Supporting Information may be found in the online version of this article:

Figure S1. Predicted minus observed ice thicknesses for the present-day ice-sheet reconstruction of Whitehouse et al. (2012).

Figure S2. (a) Plan view of grounding line retreat superimposed upon the 20 km grid. The three grounding line regions are labelled in red (see text). The blue arrow indicates the direction of grounding line retreat between time t ka BP and time $(t - 5)$ ka BP. The red dot indicates node j , the green dots indicate the closest nodes in regions $\varphi = 2$ and $\varphi = 0$. d_{2j} and d_{0j} are the distances between these nodes and node j , respectively. (b) Side view of ice surfaces during grounding line retreat between time t ka BP and time $(t - 5)$ ka BP. The three grounding line regions are labelled in red. The darkest and lightest solid blue lines indicate the ice surface derived from the numerical ice sheet model at times t and $(t - 5)$ ka BP, respectively. The mid-blue solid line indicates the position of the intermediate ice surface at $(t - 2.5)$ ka BP. The dashed lines indicate the ‘target’ ice thickness (see text) at the intermediate time (mid-blue) and $(t - 5)$ ka BP (light blue). d_{2GL} and d_{0GL} are the distances used to define the ratio $(d_2/d_0)_{GL}$, which is used to test whether a node lies inside or outside the grounding line. (c) Side view of the ice surfaces during grounding line retreat if the ‘target’ ice thickness at the intermediate time is assumed to be zero rather than the thickness of ice at flotation.

Table S1. Details of the 16 ice-sheet reconstructions used in Experiment 3 (see main text). The values in italics define the ‘best’ deglaciation history of Whitehouse et al. (2012); this is the model that we call W12. D is lithospheric rigidity and τ is asthenospheric relaxation time, as described in the Glimmer ice-sheet model (Rutt et al. 2009). The spatially variable sea surface height is derived using the ICE-5G global deglaciation model (see Whitehouse et al. (2012) for further details).

Table S2. Details of the GPS sites used in this study together with the observed, modelled elastic, and elastic-adjusted vertical GPS rates, modelled vertical GIA rates, and the misfit between modelled and observed (elastic-adjusted) vertical rates (positive denotes uplift). One sigma uncertainties are given (see Thomas et al. 2011), and the method used to model the elastic rates is described in Thomas et al. (2011). At nine locations with co-located receivers, individual site rates are not used (grey); rather, weighted average rates are derived to give the ‘AV’ rates (bold). At the Northern Antarctic Peninsula sites, the starred (*) records are the rates used in the analysis as the best estimate of the viscous GIA signal. These are derived from pre-March 2002 data: the elastic signal prior to the breakup of Larsen-B Ice shelf is assumed to be close to zero at these locations. The subsequent entries for these sites are given the suffix ‘EL’ where the GPS rates are derived from the post-March 2002 data and are dominated by the elastic signal associated with the glacier speedup after the Larsen-B break up. The modelled GIA rates are generated using the W12 and W12a deglaciation models with the optimum earth model (see main text), as plotted in Figs 10(b) and (d) of the main text.

Supplement. Material that is critical to understanding the development of the new glacial isostatic adjustment (GIA) model is included in the main text. Here we present highly specialized details, which are only likely to be of interest to those seeking to perform a similar study.

Please note: Wiley-Blackwell are not responsible for the content or functionality of any supporting materials supplied by the authors. Any queries (other than missing material) should be directed to the corresponding author for the article.